(F) ACCURACY OF NUMERICAL RESULTS BASED ON AN
ASYMMETRIC NETWORK

1. Problems Studied and Network Used.

To further investigate the effect of asymmetry on the accuracy of the approximation solutions, the numerical results for the transient problem used in Chapter III, section D, and for the steady-state problem mentioned in section C of this chapter can be studied and compared with their corresponding continuous solutions. Both of these approximate calculations are based on the asymmetric network in Figure III-1.

The transient problem is described in Chapter III, section D. Briefly, a solid with a unit square cross-section is initially at a unit temperature, and at time zero the surfaces are held at zero temperature. This problem is important as the eigenvalues and eigenfunctions for this problem are the same for any transient problem in the unit square with a different initial temperature distribution and with surface temperature a function of space and time; hence, the accuracy with which the asymmetric approximation solves the above transient problem is an indication of the accuracy of the transient part of the approximate solution. In this problem only the triangular one-eighth of the cross-section bounded by $\xi = 0$, $\xi = -\eta$, and the surface, $\eta = -\frac{1}{2}$,

as shown in Figure III-1, need be used, because the temperature

distribution is always symmetric about both the hypotenuse ($\xi = -\eta$)

and the vertical boundary ($\xi = 0$). Thus, the problem can be considered

to be just the triangle with the surfaces at $\xi = 0$ and $\xi = -\eta$ adiabatic,

and the surface at $\eta = -\frac{1}{2}$ at zero temperature. The details of the

approximate transient calculation are given in Chapter III, and the

continuous solution is given by equations III-34 and III-35.

The steady-state problem has been described in section C of

this chapter. It is to find the steady-state temperature distribution in

a unit square with its horizontal surfaces at unit temperature and its

vertical surfaces at zero. The steady-state solution is the remaining

part of the complete solution for the problem of transient temperature

distribution; the complete continuous or approximate solution actually

is often found by finding the transient and steady-state parts separately

and then adding them (see Chapter II and reference (1)). Thus, the

results of this study can be used as an indication of the accuracy of

the steady-state part of the approximate solution. Further, the errors

in this solution are a direct result only of the space discretization

error; and hence, this study gives an understanding of the practical

effect of zero-order error terms in the expansion for the space dis-

cretization error. The continuous solution of this problem is given in

equation V-32. The temperature distribution for this problem is sym-

metric about the vertical ($\xi = 0$) axis and anti-symmetric about the

hypotenuse $(\xi = -\eta)$. Therefore, again, only the 1/8-cross-section used in Figure III-1 need be considered, as a problem with the surface at $\xi = 0$ adiabatic, the hypotenuse $(\xi = -\eta)$ at a temperature of $\frac{1}{2}$, and the surface at $\eta = -\frac{1}{2}$ at unit temperature.

The arrangement of points used for both problems is shown in Figure III-1. This arrangement was deliberately made very irregular so that the effects of asymmetry could be studied and it is far from the optimum, which would probably be a network of squares. Further, the network contains only 8 or 9 points at which the temperature is to be found; this is an extremely coarse network equivalent to about 3 points for a one-dimensional problem.

The surfaces of the triangle are described by the two types of nodes; the first, located on the $\eta = -0.5$ boundary, follows MacNeal's rules by being on the boundary. However, the nodes along the vertical boundary and the hypotenuse, except for node 9, are located inside the solid so that part of the boundary of the nodes follows the boundary of the solid, rather than the node being located on the surface boundary. The location, calculation of the conductances and capacitances, and the advantage of this type of node are discussed in the next section.

Although the arrangement of the points for the two problems is the same, the Y matrices are different because of the different boundary conditions along the hypotenuse. In the transient problem the heat-transfer coefficient is zero, but it is infinite in the steady-state problem.

Thus, the Y matrix for the transient problem is 9 x 9, but because

the temperature at node 9 is specified in the steady-state problem it

is fixed at $\frac{1}{2}$ and the Y matrix for the steady-state problem is 8 x 8.

However, the approximation is in reality the same for each problem.

This can be seen by considering the square which is $\frac{1}{4}$ of the original

square rather than the triangular 1/8. Now all that has been changed

is boundary temperatures, which do affect the coefficients of the

derivatives in the expansion for the discretization error.

2.   Transient Problem.

The approximate solution to the transient problem was stepped

out for each of several time increments for each of the most common

values of the weighting factor of γ, of 0, $\frac{1}{2}$, and 1. Table V-10 is an

abstract of errors for each of the nine points at 6 times for several

different combinations of the time differencing parameters. The

results at temperature points 1 and 6 were studied in more detail

for only four combinations of time differencing parameters. These

studies are shown in semi-logarithmic graphs for both the continuous

and approximate solutions for the temperature versus dimensionless

time. The graphs for point 1, for short, intermediate, and long times,

are in Figures V-9, V-10, and V-11, respectively; and for point 6 for

short and long times in Figures V-12 and V-13, respectively. After

determining the effect of the time differencing parameters the effect of

the space discretization errors can be studied.

Time Differencing Parameters. The solution labeled analog

solution in the table and on the graphs actually is the fourth-order

Runge-Kutta method of integration for a system of ordinary differential

equations. Three such calculations were made with time increments

of 0.01, 0.001, and 0.0001. The calculations with the last two time

increments agreed to within at least the fourth significant digit for most

points even at very early times. Because of this and because of the

reported high accuracy (18) of the Runge-Kutta methods, this calculation

was assumed to be essentially the analog solution.

Several observations can be made by studying Table V-10.

First, for all points and all times, with the exception of point 1 at short

times, the analog solution has approximately the same error as do the

difference solutions with relatively small time increments ($\Delta \tau \leq 0.0005$)

for all values of weighting factors, and difference solutions with a γ

of $\frac{1}{2}$ for time increments up to and including 0.0015. This would be

expected from the conclusions about the time differencing parameters

for the one-dimensional problem. In Chapter IV, section E-4, and

from Figure IV-15, it was concluded that the damping factors for

approximate solutions with a small time increment, for a weighting γ

of $\frac{1}{2}$, are very close to those of the analog solution. Thus, this

dependence on time differencing parameters for an approximate solution

in two dimensions would be expected, because the form of the expansion

for the time discretization error is the same for both one- and two-

dimensional approximations.

Second, the approximate solutions for the largest time increment of 0.01 for weightings γ both of $\frac{1}{2}$ and 1 show relatively large errors, although both solutions are stable. The large error in the approximate solution for a weighting of $\frac{1}{2}$ is caused by excessive oscillation (see Figure III-3). The large inaccuracies for the run with the weighting of one agrees with the conclusion in Chapter IV, section E-2, where it was shown that this weighting gives the least accurate damping factors for a fixed time increment and a fixed number of points. Note also that, of the approximate solutions that are like the analog solution, the solution with a γ of 1 and time increment 0.0005 shows the poorest agreement with the analog and also is the least accurate of the approximations.

Third, the solutions for node 6, and its neighboring nodes 4, 7, and 8, have the largest errors. Further, these errors for node 6 do not change much over a wide change in time differencing parameters. However, the errors for nodes 1, 2, and 3 are much smaller, and these errors do depend upon the time differencing parameters. This effect can be explained by the space discretization error and is discussed in the next section.

The graphs of temperature versus dimensionless time for the continuous solution and for each of several approximations are shown in Figures V-8, 9, and 10 for node 1 and in V-11 and V-12 for node 6. In the graphs the analog solution is shown and considered to be

representative of the solutions with small time increments ($\Delta\tau \leq 0.005$)

or with weighting γ of $\frac{1}{2}$. up to time increments of 0.0015. Also

shown are the two backward difference solutions with time increments

of 0.0005 and 0.01 and the forward difference solution with a time

increment of 0.001.

As shown in Figures V-8 and V-9 the continuous temperature

at node 1 decreases very rapidly with time because it is close to the

surface. This means that the smaller damping factors have a relatively

large weighting in the solution for this node and give a significant

contribution to the solution at short times. The approximate solutions

for node 1 are the most sensitive to oscillations because of this rela-

tively large weighting for the smaller damping factors. Moreover,

the significant contribution of these smaller damping factors causes

the disagreement between the approximate difference solutions and

the analog solution at short times. Probably even smaller time

increments would be required to make these smaller damping factors

agree with those of the analog solution. In Figure V-10 the temperature

at node 1 becomes linear on the semi-logarithmic paper at long times,

as expected. The behavior of the continuous and approximate solutions

at nodes 2, 3, and 4 is like that at node 1 except that the weightings of

the smaller damping factors are not as great at these nodes.

In contrast to the behavior at node 1, the continuous temperature

at node 6 remains about constant for a short time after the surface

temperature is changed, and then decreases almost linearly with time

as shown on the semi-logarithmic graph, Figure V-11. This indicates

that at most only one or two damping factor terms give a significant

contribution to the solution at node 6. The straight line behavior actually

begins when node 6 has reached a temperature of 0.65 compared to

node 1, which does not show this behavior until a temperature of 0.007

is reached. This behavior of both the continuous and approximate

solutions at node 6 is like that at nodes 5, 7, 8, and 9.

From a study of the graphs for long times the following important

observations about the straight-line portion can be made for both nodes.

The approximate solution for the backward difference calculation ($\gamma = 1$)

with a large time increment, 0.01, decreases more slowly than the

central difference calculation ($\gamma = \frac{1}{2}$) as represented by the analog

solution. The central difference calculation ($\gamma = \frac{1}{2}$) , in turn, decreases

more slowly than the explicit calculation ($\gamma = 0$) with a time increment

of 0.001. This means that the slowest-decaying damping factor, q_{MAX},

for the backward difference calculation is greater than that for the

central difference calculation which is greater than that for the explicit

calculation. From the behavior of the approximate solutions, this

ranking of damping factors probably also applies for the smaller damping

factors. This is the same dependency of the damping factors on the

weighting γ which was shown in Chapter IV, section E-4, for the

one-dimensional problem. Such a similarity in the behavior of the

damping factors and the weighting γ between the one-dimensional regular network and the two-dimensional asymmetric network would be expected because the time discretization error has the same form in both cases. Thus the conclusion can be made that the approximate transient solution for a weighting γ of 1 decays much too slowly, compared to the continuous solution, and this is the reason for its inaccuracy.

However, a discrepancy does occur between the regular one-dimensional approximation and the two-dimensional asymmetric approximation. This is that for the one-dimensional approximation the solution with a weighting of $\frac{1}{2}$ gives damping factors larger than the corresponding damping factors of the continuous solution; for a γ of zero damping factors less than the corresponding damping factors of the continuous solution are obtained; and a γ of γ_o gives damping factors very nearly equal to those of the continuous solution. However, for the asymmetric approximation even the explicit solution with a γ of zero and a time increment of 0.001 decays more slowly than the continuous solution, indicating damping factors larger than those of the continuous solution. A possible reason for this discrepancy is that the space discretization error for the network used was too large to obtain the necessary compensation with the time discretization error. The large discretization could be caused either by the asymmetry or the coarseness of the network, but most probably by the asymmetry.

Other observations based on the graphs are:

(1) The approximate solution for the explicit calculation with the relatively large time increment of 0.001 oscillates too wildly at node 1 at short times to be useful. However, for node 1 at long times and node 6 it is one of the most accurate solutions.

(2) The implicit calculation with γ of 1 and a large time increment of 0.01 is inaccurate almost all of the time.

(3) The approximate solutions that give results equivalent to the analog solution give reasonably accurate solutions despite the coarseness and asymmetry of the network. The important calculation in that group of approximations is the one with γ of $\frac{1}{2}$, which does not require too small a time increment to give an approximation close to the analog.

Selection of Time Differencing Parameters for an Asymmetric Network. The numerical results obtained above and the form of the time discretization error are very much alike for both the one-dimensional regular mesh and the two-dimensional asymmetric network. Consequently, the rules for selecting the time differencing parameters are also similar. However, since there does not appear to be a specific optimum weighting, γ_o, for the asymmetric network, the accuracy restriction is somewhat arbitrary, and it is suggested that the weighting γ not be larger than $\frac{1}{2}$. It should be pointed out that, for the asymmetric network above, using any weighting other than zero increases

the errors, and the weighting factors that give the most accurate q_{MAX} are negative. Thus, using a large weighting factor, approaching one, for an asymmetric network can introduce significant errors.

The oscillatory restriction that assures that the maximum oscillatory contribution is less than V at the initial time of interest is found by writing equation IV-295 for an arbitrary minimum matrix norm, M:

$$V >> \Phi(\underline{v})^{\tau_0/\Delta\tau} = \Phi\left[\frac{M(1-\gamma)\Delta\tau - 1}{M\Delta\tau - 1}\right]^{\tau_0/\Delta\tau} \qquad (V-81)$$

Thus, using this equation, the allowable time increments for a fixed network of points with γ's of 0 and $\frac{1}{2}$ can be found; also, the weighting γ can be found which will allow the use of the minimum practical time increment.

In order that an implicit solution involve less time-consuming calculation than the explicit solution, the ratio of the time increment for the implicit solution to that for the explicit must satisfy the following relationship,

$$\frac{\Delta\tau_{Im}}{\Delta\tau_{Ex}} > \frac{5U + 2S + \sum\limits_{i=1}^{S} u_i^2}{2U + S} \qquad (V-82)$$

where U = total number of off-diagonal elements above diagonal in

$$Y/A \text{ matrix} = \sum_{i=1}^{S} u_i$$

and u_i = number of off-diagonal elements above diagonal in i^{th} row

in Y/A matrix

This is based on the number of non-zero multiplications required to advance one time increment where the implicit calculation is carried out according to the elimination method discussed in Chapter III, section E. If u_i does not change much from node to node, the summation of the u_i^2 terms can be approximated by

$$\sum_{i=1}^{S} u_i^2 \simeq \bar{u} \, U \tag{V-83}$$

where $\bar{u} = \left(\sum_{i=1}^{S} u_i \right)/S$ = one-half the average number of nodes that surround each node in the network.

If a rectangular network is used, a node has four neighbors, u_i is two, and the relationship becomes:

$$\frac{\Delta\tau_{Im}}{\Delta\tau_{Ex}} > \frac{16}{5} = 3.2 \tag{V-84}$$

If the network contains equilateral triangles, each node has 6 neighbors, and u_i is three; the ratio becomes:

$$\frac{\Delta \tau_{Im}}{\Delta \tau_{Ex}} > \frac{26}{7} = 3.72 \qquad (V-85$$

For most asymmetric networks the average $\bar{u}$ is probably somewhere between two and three and thus $\Delta \tau_{Im}$ must be somewhat larger than about $3.5 \Delta \tau_{Ex}$ for the implicit calculation to be more efficient. This is the same ratio found for one-dimensional problems with a regular mesh where vector-matrix multiplication is not used (equation IV-305).

Based on these results, it is probable that for most asymmetric networks the weighting γ of $\frac{1}{2}$ should be used with a time increment about the maximum given by equation V-81. Although this might not give the most accurate solution possible with the specific network, in all probability it should give reasonable accuracy with no significant oscillations, and should require about the minimum calculations.

Space Differencing Parameters. One of the effects on the approximate transient solution, which is probably attributable to the asymmetric location of the temperature points, is that the eigenvalues of the Y/A matrix are sufficiently different from the eigenvalues v_j^2 of the continuous problem, so that the damping factors of the approximate solution are greater than those of the continuous solution for any reasonable combination of weighting and time increment.

The other inaccuracy in the transient solution caused by the space discretization error, as indicated in Chapter II, section D, and Chapter IV, section E-2, is the error in the intercepts of the transient

terms, when plotted versus time on semi-logarithmic paper. This

difference is $(a_j b_{ij} - g_j c_{ij})$. On the long-time plot for nodes 1 and 6,

Figures V-10 and V-12, the straight-line portion is extrapolated to

zero time to find the intercept corresponding to the maximum damping

factor for both the continuous and approximate solutions. This shows

that the error in this quantity is much larger for node 6, about 0.09,

or about 10 per cent error, compared to 0.01, or about a 3 per cent

error, for node 1. Further, since in both of the approximate intercepts

the quantity g_1 is the same for both nodes, the larger error for node 6

is caused by the fact that its component c_{61} in the first eigenvector is

more in error than the corresponding component c_{11} for node 1.

Moreover, none of the approximate solutions for node 6 give the very

slow changes in temperature for very short times ($\tau < 0.005$) in com-

parison with the analog solution for node 1 which is relatively close

to the continuous solution. This indicates that the intercepts for node

6, $g_j c_{6j}$, for the remaining terms in the approximate solution are quite

inaccurate, but that the corresponding intercepts for node 1, $g_j c_{1j}$,

are accurate. In both cases, much of the difference in accuracy must

be due to the fact that the elements in row 6 of the eigenvector matrix

do not agree with the eigenfunctions evaluated at node 6; but row 1 in

the eigenvector matrix agrees with the first several eigenfunctions

evaluated at point 1. Secondary reasons for the higher accuracy for

node 1 are that its approximate solution might contain higher weightings

of the approximate transient terms which are more accurate, and that
errors in the several terms which are significant at short times might
compensate.

The relative accuracy and behavior of the transient terms for
nodes 1 and 6, and for the other nodes, can be explained qualitatively
in terms of the error propagation equation and the space discretization
error expansions with only a superficial knowledge of the derivatives.
First, the expansions for the space discretization for nodes 1 and 6
are shown in Table V-9 as nodes O and P, and these expansions have
non-zero coefficients of the zero-order error terms, which are the
hyperbolic derivative term ($\frac{\partial^2 T}{\partial \xi^2} - \frac{\partial^2 T}{\partial \eta^2}$) and the mixed derivative
($\partial^2 T/\partial \xi \partial \eta$). Examination of the network in Figure III-1 indicates that
these terms would be expected for all but node 3 which is an irregular
rectangular node with the first term in the expansion for its discret-
ization error proportional to a linear distance in the node (see node C,
Table V-9). A consideration of the symmetry of the temperature dis-
tribution or the adiabatic condition for the vertical boundary ($\xi = 0$)
and the hypotenuse boundary ($\xi = -\eta$) allows the following conclusions
about the derivatives in the zero-order error terms.

(1) The hyperbolic derivative term ($\frac{\partial^2 T}{\partial \xi^2} - \frac{\partial^2 T}{\partial \eta^2}$) is small for
nodes 1, 2, 3, 5, and 7, located close to the hypotenuse, because
$\partial^2 T/\partial \xi^2$ and $\partial^2 T/\partial \eta^2$ are the same size and have the same sign.

(These second derivatives are equal on the hypotenuse.) The mixed partial derivative in this region is probably intermediate in size.

(2) The hyperbolic-derivative terms for node 4, located very close to the horizontal surface and relatively close to the adiabatic boundary ($\xi = 0$), and node 6, located very close to the adiabatic boundary ($\xi = 0$), are large as the derivative $\partial^2 T/\partial \eta^2$ has a large absolute value, but $\partial^2 T/\partial \xi^2$ is small. The ξ derivatives are small on the vertical boundary. The mixed derivative is very small for these nodes.

(3) The space discretization error for node 9 is small because of the low rates of heat transfer from this node, and because of symmetry.

(4) Both the space and time derivatives at each node are zero at zero time and increase to a maximum value when the temperature gradients become large. This maximum value is attained at different times for different nodes, occurring at short times for nodes 1, 2, 3, and 4, but at long times for nodes 6, 7, and 8. After this maximum is reached the derivatives go to zero as the steady-state condition of a uniform zero temperature is approached.

Based on these considerations, both the discretization error $d_{i,n}$ and the averaged discretization error $\bar{d}_{i,n}$ would be expected to be relatively large for nodes 4 and 6, and relatively small for nodes 1, 2, 3, 5, 7, and 9. The larger discretization errors for node 4 should occur at short times; the larger discretization errors for node 6 occur at somewhat longer times. As discussed previously, and as seen from

equation V-22, the discretization error associated with each node is now multiplied by the node's area to find the area-weighted averaged discretization error vector elements $A_i \bar{d}_{i,n}$. The elements in this vector, although less in absolute value than those in $\bar{d}_{i,n}$, are increased for the large nodes 4, 5, 6, 7, and 8 relative to the size of errors at the small nodes 1, 2, and 3. This is particularly true for the weighting at node 6 because it has the largest area of any of the nodes.

The quantities which are the relative weighting of the area-weighted discretization error in the error at each point are the elements in the inverse conductance matrix Y^{-1}. This matrix is in Table V-1. It shows that the large discretization error for node 4 at short times should contribute more to the error at nodes 4, 5, 6, 7, 8, and 9, than at nodes 2 and 3, and it should contribute almost insignificantly to the error at node 1. The errors in Table V-10 indicate qualitatively that this is true. The errors for dimensionless times of 0.003 and 0.006 are largest for nodes 4 and 6; the next larger errors at nodes 2 and 3 are probably caused by discretization errors at those nodes in addition to the contribution from node 4. Further, the error at node 4 is almost independent of the time differencing (except for the oscillatory run, $\gamma = 0$, $\Delta\tau = 0.001$), indicating that its discretization error is mostly caused by the space differencing parameters. On the other hand, node 1, despite its asymmetry, has a very accurate solution, because it is not affected by nodes other than 2 and 3, which probably have a low discretization error.

At intermediate and long times the discretization errors at nodes 1, 2, 3, and 4 become very small and most of the approximate solutions become accurate at these nodes. However, the space discretization error at node 6 is now large and because of its large area this discretization error contributes to the large error in its own approximate solution, and to the errors of nodes 5, 7, 8, and 9. In particular, node 9 is known to have a very small space discretization error, and yet its solution is not accurate, because of the dominant effect of the large area-weighted discretization error at node 6, $A_6 \bar{d}_{6,n}$.

3.   Steady-State Problem.

In the steady-state problem only the space discretization errors need be considered and only for one time. The analysis of the effect on the errors in the approximate steady-state solution follows much the same pattern as above. In the transient problem just discussed, the temperatures approach a constant value throughout the solid and the discretization error, and hence the error in the solution approaches zero with time; however, in the steady-state problem, the boundary conditions are such that the temperature distribution is very non-uniform. This problem was selected particularly because of this non-uniformity, as a test of the space discretization error.

As pointed out previously, despite the radically different boundary condition along the hypotenuse, $(\xi = -\eta)$, the coefficients of the derivatives in the expansion for the space discretization error are the same

as for the transient problem; however, the values of the derivatives at the several nodes are radically changed. As this is a steady-state problem the continuous temperature distribution satisfies Laplace's equation and the hyperbolic derivative becomes

$$\frac{\partial^2 T}{\partial \xi^2} - \frac{\partial^2 T}{\partial \eta^2} = 2\frac{\partial^2 T}{\partial \xi^2} = -2\frac{\partial^2 T}{\partial \eta^2} \qquad (V-86)$$

Consequently, the hyperbolic derivative is very large in regions of high net energy flow in the ξ or η direction. From a consideration of the boundary conditions, one such area is the corner where nodes 1, 2, and 3 are located. In this region the mixed second partial derivative is large also. Thus, nodes 1 and 2, which contain these terms in their expansions, would be expected to have very large space discretization errors. The expansion for node 3 is given as node C in Table V-9, and although the zero-order error terms are not present, the third derivatives are also high, as can be seen by writing the expansion for the steady-state problem at node 3 as

$$\sigma_{3,SS} = 0.118\,\frac{\partial^2 T_{3,SS}}{\partial \xi'^2} + 0.0115\,\frac{\partial^3 T_{3,SS}}{\partial \eta'^3} + \ldots \qquad (V-87)$$

where ξ' is perpendicular to the hypotenuse and η' is parallel to the hypotenuse. Although the third derivative along η' is small, the one along ξ' perpendicular to the hypotenuse is large and causes the discretization error at node 3 to be large. This is true even though the

expansion for node 3 contains no zero-order error terms.

The discretization error would be expected to be decreased as one moves along the hypotenuse toward the origin; thus, the discretization errors for nodes 5, 7, and 8 should be significantly smaller than those for nodes 1, 2, and 3. Node 5 would be expected to have a larger discretization error than nodes 7 and 8.

On the other hand, at node 6, not close to either boundary of specified temperature, but located close to the adiabatic vertical boundary ($\xi = 0$), the second partial derivative $\partial^2 T / \partial \xi^2$ is much smaller than in the corner region. The mixed second partial derivative is also smaller, and it would be expected that the higher-order derivatives are also small. Consequently, the space discretization error at node 6 should be small.

The space discretization error for each of nodes 1 to 8 has been calculated directly from the definition of this error, equation V-4, using the continuous solution temperatures, as computed from equation V-32. These results are summarized in Table V-7 (1) for the case when the boundary temperature vector is taken as the continuous boundary temperature vector. A study of the space discretization error $d_{i,SS}$ does indeed confirm the qualitative expectations mentioned above. That is, nodes 1, 2, and 3 have very large discretization errors compared to node 6, and larger errors than nodes 5 and 7. Node 2 has a significantly smaller discretization error than 1 and 3, as it is located somewhat farther from the hypotenuse. Node 4 has a large error as

it is located close to a region where $\partial^2 T/\partial\xi^2$ is high, due to the

closeness of the boundary with a specified temperature (ξ = -0.5).

Consequently, we conclude that the series expansions for the space

discretization errors are valid, and, more importantly, that, with only

a very superficial knowledge of the expected temperature distribution

or its derivatives, the relative size of the space discretization error

can be predicted.

The discretization errors shown in Table V-7 for the nodes in

Figure III-1, with the temperature distribution of the steady-state

problem, are much larger than the errors shown for nodes J and L

in Figures V-5 and V-6, for a steady state which is similar to that

under consideration here. There are two reasons for this. First,

nodes J and L were located on the semi-infinite solid on the vertical

axis of symmetry and fairly well into the interior, which would cor-

respond roughly, for the problem considered here, to a point located

at ξ = 0 with the same η coordinate as node 6. Thus, these nodes

are positioned at a point where the derivatives are small rather than

at the corner where the derivatives must be large. Second, if the two

problems had their space dimension scaled in the same way, the

largest dimension λ for nodes J and L would correspond to about

0.03 instead of 0.10 as shown. Thus the largest nodes J and L have a

dimensionless area of 0.0009 compared to the areas of the nodes in

Figure III-1, which range from 0.0034 to 0.0242, and the calculations

for J and L are for nodes in a much finer network.

The area-weighted discretization error $A_i d_{i,SS}$ and the errors in the approximate solutions $v_{i,SS}$ are also shown in Table V-7. The area weighting of the discretization error for the small nodes 1, 2, and 3 reduces the large discretization error relative to the area weighting of the discretization errors at the larger nodes. This area-weighted discretization error is largest for nodes 1 and 4; and this error at nodes 2, 3, and 5 is significantly larger than at 6, 7, and 8. The error in the approximate solution for the ith node is found by multiplying each $A_j d_{j,SS}$ by the jth element in the ith row of the inverse conductance matrix. This matrix is in Table V-2. In general, those nodes in a region with high discretization errors should have the largest errors in their approximate solution; nodes with smaller discretization errors should have more accurate solutions, if they do not have large conductances to a large area with large discretization errors.

These results are confirmed in Table V-7, which shows larger errors at nodes 1, 2, 3, and 4, than at 5, 6, 7, and 8. The approximate solution for each point, if rounded to two significant digits, would agree, within a difference of one in the last digit, with the continuous solution, similarly rounded; this is true despite the large discretization errors caused by the asymmetry and the coarseness of the network. This surprisingly good agreement is partially accounted for by the

compensation caused by the discretization errors having different

signs, and by the Y^{-1} matrix containing only negative elements.

4.   Summary of Conclusions--Numerical Studies.

The conclusions that can be made based on the numerical results

for the transient and steady-state problems are:

(1) In spite of the coarseness and the asymmetry of the network,

both the approximate transient solution and the approximate steady-

state solution are reasonably accurate. This means that the eigenvectors,

eigenvalues, and the resulting initial vectors for an asymmetric dis-

tribution of points can be of reasonable accuracy.

(2) The relative accuracy of these solutions at different points

and at different times is at least qualitatively predictable on the basis

of the series expansions for the discretization error and a consider-

ation of the quantities in the equation for the propagation of this error.

This can be done by considering the derivatives for the expected tem-

perature distribution, and the relative areas and conductances between

the points.

(3) The error in the approximate solution for each point in a

fixed network is largely dependent on the second- and higher-order

space derivatives for the specific temperature distribution being

approximated. That is, a network which gives an accurate approximate

solution for nodes in a certain region for one problem might give a

rather inaccurate solution for another problem, where the temperature distributions are different.

(4) The time differencing parameters, time increment and weighting factor γ, influence the approximate solution based on an asymmetric network about as they do for a one-dimensional problem with a regular network. In selecting these parameters for a fixed network of points, the oscillatory criteria probably limit the size of time increment that can be used. The weighting factor γ should probably not be much greater than $\frac{1}{2}$, if accuracy is important, but the solution for a γ of $\frac{1}{2}$ should give an adequately accurate solution.

(G) RULES FOR LOCATING A LIMITED NUMBER OF POINTS

Because Richtmyer's consistency condition is based on how the discretization error changes as the network is refined, it is not directly useful in many practical situations where the network contains only a limited number of points. Although networks of 100 to 1000 points in each space coordinate direction have been suggested by Forsythe and Wasow (10), to obtain moderate or fine detail, in most practical cases approximate solutions of adequate engineering accuracy can be obtained with a coarse mesh of less than thirty points. Furthermore, computers that can handle such a large number of points are not always available. In simulation problems, where the transient temperature distribution calculation is only a part of the total calculation, only part of the memory capacity of the computer is available for the transient calculation, and the time allowed for the calculation might also be limited. Consequently, even with the large high-speed computers currently in use, approximate methods which do not require a large number of points are important practical tools to obtain solutions that are of sufficient accuracy for engineering purposes.

In these cases, where a relatively coarse network of less than thirty points is to be used, the accuracy of the approximation is affected by the discretization errors of the network to be used, and the way in which the discretization changes as more points are added is not

of practical significance (unless these points are actually added).
Consequently, the expansion for the discretization error (equation V-57)
is important in this situation because it allows an estimate of the
discretization error with only a minimal knowledge of the temperature
distribution. Further, for a relatively coarse network, the first- and
second-order error terms can be as large as the zero-order term; and,
since the network is not to be refined, the zero-order term has no
special significance. The primary concern is the space discretization
error, which is the sum of all terms. Moreover, the numerical results
just discussed show that solutions of reasonable accuracy can be
obtained with a coarse asymmetric network that is probably very dif-
ferent from the best network for the problems approximated. In the
light of the above remarks, and also the numerical results, a properly
selected asymmetric network used to describe a solid with irregular
boundaries should not be rejected merely because series expansions
based on Cartesian coordinates for some nodes in the network contain
a zero-order error term.

The following is a summary of several general rules on locating
nodes in a solid with irregular boundaries and, possibly composed of
materials of different thermal properties. The rules assume that
MacNeal's rules are to be used in locating the points and in calculating
the conductances; however, on the basis of the results of Chapter IV,
a modification is proposed to the location of the points that follow the

curved boundary. In most instances the rules are based on physical considerations or mathematical analogies rather than rigorous mathematical proofs. The discussion is divided into two parts; one on the location of the adjacent nodes that describe the boundary; and one on the location of the interior points within the solid.

It should also be pointed out that because of the general nature of the problems that can occur, and the usual lack of all but a superficial knowledge of derivatives, these rules cannot predict quantitatively the error for a fixed network, or how many points are necessary to obtain a certain desired accuracy. However, a qualitative estimate of the expected relative accuracy can be obtained, based on an analysis like that used in the discussion of the numerical results. A quantitative study would require a series expansion for the discretization error and quantitative estimates of the derivatives at each node. Thus, in the following discussion, the maximum number of points that can be used is assumed to be relatively small and known. The average area for each node in a uniform solid can then be estimated by dividing the total area of the solid by the number of nodes. The average distance between nodes can be estimated by taking the square root of this number.

1.   Location of Adjacent Nodes.

MacNeal's original idea of the asymmetric network was to follow a curved or irregular boundary by actually locating the points on the

boundary. The argument for this is that any errors introduced by the resulting asymmetry are expected to be less than the errors caused by making the solid boundary conform to a regular network or other approximation. Locating the points on the boundary is a generalization of method G based on mesh $\Delta\xi$ for the one-dimensional problem; hence, this technique is subject to the same disadvantages that are associated with method G. A method of following the boundary exactly, but locating the nodes a short distance inside the boundary, is suggested. This location of the adjacent nodes is a generalization of the one-dimensional method C based on mesh $\Delta\xi/2$, and it is shown to preserve the advantages of method C.

Two types of boundary conditions are discussed separately. The first is the heat-transfer coefficient condition given by equation V-42. This equation applies to the external surfaces of the solid which are exposed to the fluid. Since the heat-transfer coefficient is allowed to vary from zero to infinity inclusive, this condition includes the adiabatic boundary condition, and the specified temperature boundary condition. The second type of boundary equation considered is the interface boundary condition between two solids of different uniform thermal properties in a composite solid. This condition assumes perfect thermal contact:

$$k_I \frac{\partial T_I}{\partial \eta} (\xi_i, \eta_i, \tau) = k_{II} \frac{\partial T_{II}}{\partial \eta} (\xi_i, \eta_i, \tau) \qquad \text{(V-88)}$$

and

$$T_I(\xi_i, \eta_i, \tau) = T_{II}(\xi_i, \eta_i, \tau) \qquad \text{(V-89)}$$

where $T_I(\xi_i, \eta_i, \tau)$ = temperature of solid I with thermal conductivity

I evaluated at the interface with solid II,

and $T_{II}(\xi_i, \eta_i, \tau)$ = corresponding function for solid II.

Fluid Boundary Condition. $0 \leq h \leq \infty$. The disadvantage of

locating the points directly on a boundary surface in contact with a

fluid, as shown in Figure V-1, are:

(1) Heat capacity is associated with the boundary surface tem-

perature in the approximate method, but no heat capacity is associated

with the surface in the continuous formulation; consequently, the

approximation is not a direct discretization of the continuous boundary

condition, equation V-42.

(2) For infinite heat-transfer coefficient, some heat capacity

of the solid is neglected.

(3) For very large heat-transfer coefficient, heat capacity of

the surface node must be neglected, or the stability and non-oscillatory

criteria become very restrictive because the minimum norm M of the

Y/A matrix is directly proportional to the heat-transfer coefficient.

All of the above objections can be avoided and the curved boundary followed exactly if the adjacent nodes are located a short distance inside the surface rather than on the surface. This gives a generalization of method C based on mesh $\Delta \xi / 2$.

A portion of such a network is in Figure V-13. This can be constructed easily by first drawing a curve that is approximately parallel to the boundary and inside the boundary by about half the average distance between nodes. The adjacent nodes are then located on this curve. From each of these adjacent nodes a line normal to the boundary is drawn. The interior nodes can be located, and the network and perpendicular bisectors constructed, in the usual manner.

The equation for the adjacent nodes is based on an energy balance on the area bounded by the perpendicular bisectors and a portion of the boundary of the solid. This area is cross-hatched for the ith node in Figure V-13, and it is the area used for the heat capacity. (The feature that distinguishes this type of adjacent node from interior nodes is that a boundary of the adjacent node is also the boundary of the uniform solid.) The energy into the node from the fluid at temperature $t_{f_i, n}$ can be found by using the concept of thermal resistances. The resistance between the fluid and the surface of the solid is $1/A_{f_i} h$, and between the surface and the node is $\ell_{i, f_i} / A_{f_i} k$. The conductance between the node and the fluid is then the reciprocal of the sum of these two series resistances, divided by k_0 to make the expression dimensionless.

$$Y_{i,f_i} = \frac{A_{f_i}}{k_0} \left[\frac{1}{\frac{1}{h} + \frac{\ell_{i,f_i}}{k}} \right] \qquad\qquad (V-90)$$

Use of this dimensionless conductance, together with other dimension-less conductances found in the usual way and the dimensionless heat capacity found using the area bounded by the perpendicular bisectors and the solid boundary, gives all the elements in the Y/A and Y_B/A matrices in the row of the ith adjacent node. This energy balance is shown in Figure V-13 in dimensional coordinates. Comparison between the equation above for the dimensionless conductance and the derivation for mesh $\Delta\xi/2$, equation IV-32, shows that this formulation is analogous to method C, where A_{f_i} is one and ℓ_{i,f_i} is $\Delta\xi/2$. The conductance to the fluid temperature approaches a constant value as the heat-transfer coefficient goes to infinity.

$$\lim_{h\to\infty} Y_{i,f_i} = \frac{A_{f_i} k}{k_0 \ell_{i,f_i}} \qquad\qquad (V-91)$$

whereas equation V-2 shows that the analogous conductance for Mac-Neal's boundary nodes goes to infinity as h goes to infinity. Thus, the minimum norm M of the Y/A matrix does not become large, and, when only modified adjacent nodes are used, the minimum norm of the Y/A matrix approaches a constant as h becomes large and does not give

restrictive stability conditions. Moreover, even for an infinite heat-transfer coefficient no heat capacity of the solid is neglected. The conductance in equation V-91 goes to zero when h is zero, and thus, the modified adjacent nodes are suitable for adiabatic boundaries.

If the temperature of the solid boundary opposite the ith adjacent node must be known it can be found from the following equation, which is derived using thermal resistances.

$$t^{*}_{i,n} = \frac{\dfrac{h \ell_{i,f_i}}{k} t_{f_i,n} + t_{i,n}}{\dfrac{h \ell_{i,f_i}}{k} + 1} \qquad (V-92)$$

where t^{*}_{i} = surface temperature opposite the ith adjacent node.

The asterisk means that this surface temperature is not associated with a heat capacity, and it does not add a degree of freedom to the approximate calculation. Rearranging, this equation results in

$$h(t_{f_i,n} - t^{*}_{i}) = k \left[\frac{t^{*}_{i,n} - t_{i,n}}{\ell_{i,f_i}} \right] \qquad (V-93)$$

which is a direct discretization of the continuous boundary condition, equation V-42.

It appears that this modified type of adjacent node can be made to follow the boundary exactly and the conductances and capacities are

as easily calculated as for the MacNeal adjacent node. In addition,

such nodes meet all the objections raised about the nodes located on the

boundary. Specifically, the advantages are:

(1) They give an equation which is a direct discretization of

the boundary condition equation for a heat-transfer coefficient or for an

interface with a second uniform solid.

(2) They can be used for all values of heat-transfer coefficient

from zero to infinity, inclusive, directly without neglecting any of the

heat capacity of the solid and, of equal importance, without causing

restrictive stability conditions.

In addition to these two advantages, and on the basis of the

comparison between methods G and C in Chapter IV, we would expect

approximations using these modified nodes to be more accurate than

those where the nodes are on the boundary. Even without this expectation

of accuracy, the less restrictive stability conditions that result when

the adjacent nodes are located away from the boundary would justify

their use. This technique is one of the simplest for obtaining a good

non-oscillatory solution for many problems without using a very small

time increment or a value of γ that is so large that it introduces inac-

curacies.

In order to show that a more accurate approximation results

from using adjacent nodes which follow the boundary, and which are

located away from the boundary, we would require valid series expansions for the discretization error for these nodes. This has not been done.

Interface Boundary Condition. The location of a MacNeal node on the interface between two uniform solids is shown in Figure V-14. From a generalization of his rules, the dimensionless heat capacity of the interfacial node is

$$A_i = \frac{(\text{Area})_{i\,I}\,\sigma_{II}C_{p\,I} + (\text{Area})_{i\,II}\,\sigma_{II}C_{p\,II}}{\sigma_0 C_{p\,0}\,L^2} \qquad (V-94)$$

where the $(\text{Area})_{i\,I}$ is an area within the polygon of perpendicular bisectors of solid I with thermal properties subscripted by I and $(\text{Area})_{i\,II}$ is the corresponding area for solid II. The conductance to other nodes on the interface is assumed to be the sum of two parallel conductances, one in each solid:

$$y_{i\,1} = \frac{r_{i,1\,I}\,k_I + r_{i,1\,II}\,k_{II}}{k_0\,\ell_{i,1}} \qquad (V-95)$$

where $r_{i,1\,I}$ is the length of perpendicular bisector of $\ell_{i,1}$ within solid I, $r_{i,1\,II}$ is the length of this perpendicular bisector in solid II, and $\ell_{i,1}$ is the distance between the nodes, as usual. The conductances to neighboring nodes wholly within either solid are computed in the usual manner, equation II-26.

This type of adjacent node for an interfacial boundary, like the same type for a fluid boundary, associates a heat capacity with the interfacial temperature, which the continuous formulation does not, and does not give a direct discretization of the boundary equation V-88. Another disadvantage of this type of node can be seen from Figure V-15, which relates the temperature along the normal to such an interface versus the normal distance for two solids with widely different thermal conductivities. Solid I, with the high conductivity, shows a relatively slowly changing temperature with distance, but the temperature in solid II, with a low conductivity, changes very rapidly, particularly at the boundary. In such a situation the temperature of a node at the interface cannot accurately represent the average temperature of its surrounding area, because of the discontinuity of the temperature distribution.

Both of the above objections can be eliminated by locating the nodes away from the interfacial surface. Such a location gives a direct discretization of equation V-88, allows an interfacial temperature to be calculated from thermal resistances (no heat capacity), and each node contains material of uniform thermal properties. A portion of a network for an interfacial boundary is in Figure V-16. The adjacent boundary nodes, i and i', for each solid are located on a common normal ii' to the interface. The conductance between them is found by taking two thermal resistances in series:

$$y_{ii'} = \frac{A_{ii'}}{k_0} \left[\frac{1}{\dfrac{\ell_{iI}}{k_I} + \dfrac{\ell_{i'II}}{k_{II}}} \right] \qquad (V-96)$$

where $A_{ii'}$ is the length of interfacial arc bounded by the perpendicular

bisectors, ℓ_{iI} is the distance along the common normal from node i

in solid I to the interface, and $\ell_{i'II}$ is the corresponding distance for

node i' in solid I. The heat capacity for each node, i and i', is based

on the area bounded by the perpendicular bisectors and the interface.

The conduction to the other neighboring nodes is found in the usual

manner. The interfacial temperature, as found by linear interpolation

using thermal resistance, is

$$t_{ii'}^{*} = \frac{\dfrac{k_I \, t_{iI}}{\ell_{iI}} + \dfrac{k_{II} \, t_{i'II}}{\ell_{i'II}}}{\dfrac{k_I}{\ell_{iI}} + \dfrac{k_{II}}{\ell_{iII}}} \qquad (V-97)$$

This expression can be rearranged to give an expression which is a

direct discretization of equation V-88.

$$k_I \left[\frac{t_{iI} - t_{ii'}^{*}}{\ell_{iI}} \right] = k_{II} \left[\frac{t_{ii'}^{*} - t_{i'II}}{\ell_{i'II}} \right] \qquad (V-98)$$

Thus, each adjacent node contains only material of uniform thermal

properties, and a direct discretization of equation V-88 is obtained.

However, a disadvantage does occur for adjacent nodes that are located away from an interface. In order that the perpendicular bisectors of the network legs between adjacent nodes meet at a common point on the interfacial surface (e.g., point C in Figure V-16), the network surrounding the interface must be of isosceles trapezoids, which are the most general quadrilaterals for which this can occur. (Some networks other than of isosceles trapezoids can be made, in principle, but their construction is more difficult.) This network can be constructed by drawing normals to the interfacial boundary at selected intervals. Then, after an i and corresponding i' are selected for one normal, the rest of the nodes can be located by drawing a line from i to the normal next to it on the boundary, so that the angle of intersection with this normal is the same as with the first normal. A line parallel to this is then drawn for node i'. The nodes on the next normal are thus located, and the trapezoidal network can be constructed surrounding the interface. In closing this network, the position of a normal can be changed by trial and error. If the perpendicular bisectors do not intersect at a common point on the interface, then the series resistances could be multiplied by different arc lengths. This would be equivalent to multiplying the left side of equation V-98 by $A_{i\,I}$ and the right side by $A_{i'\,II}$, where $A_{i\,I}$ is the length of arc bounded by the bisectors for solid I, and $A_{i'\,II}$ is the same for solid II. However, this node location now obviously no longer has the advantage of giving

a direct discretization of the boundary conditions; the advantage of having no discontinuities in temperature gradient within a solid remains.

Additional studies are required to show whether the modified adjacent nodes for interfacial boundaries would improve the accuracy of an approximate solution.

2.   Location of Interior Nodes.

The location of the points within the interior of a uniform solid obviously should be done in such a manner that the space discretization error is as small as possible for the number of points to be used, for the particular geometry and fluid temperature functions. The following is a discussion and presentation of rules and guide lines, based on the analytic and numerical studies for arranging the interior nodes. However, because of the wide range of conditions possible in problems of transient temperature distribution, exceptions to the rules do occur. Although many of the exceptions are mentioned, it is not possible to anticipate all possible situations. Consequently, these rules should be used as guide lines but not as rigid rules.

Nodes. The series expansions in Table V-9, based on Cartesian coordinates, show that any asymmetry or irregularity in dimension of an interior node probably increases the space discretization error. Asymmetry which consists in having different angles or different lengths to neighboring nodes usually results in an increase in the

coefficient of a low-order term in the series or the addition of a new lower-order term to the series. (Although at times this might produce a compensating effect, it is not assured, and is not probable.) Thus, the interior nodes should be selected from those which have only small coefficients for the second-order terms.

The best shapes are the square node E and the hexagonal node N shown in Table V-9. Both of these nodes are located at the center of the surrounding area and have equal branch lengths separated by equal angles. Nodes which have equal branch lengths in opposite directions, but unequal lengths in the two perpendicular directions, such as the rectangular node D, also are located at the centroid, and are particularly useful in problems which have much larger gradients in one direction. They can then be oriented with their short dimension parallel to the direction of highest gradient. Among other nodes like the rectangle, which have not been studied, but which should have an error expansion like the rectangle's, is a distorted hexagon (like node N) with the network shape of isosceles triangles instead of equilateral triangles. Both the irregular rectangular node C and the trapezoidal node I are not located in the center of the surrounding area; however, their error terms would still be expected to be small. The irregular rectangle is often useful in fitting irregular boundaries; the trapezoidal node is useful for radial geometry. Further, small errors probably also result from nodes that deviate only slightly, in angles or in lengths, from the type

of hexagonal nodes (node N) which form networks of equilateral triangles.

Networks. The networks in which these nodes are to be used are also restricted. Assuming a uniform solid, where the temperature gradients are fairly uniform throughout, and where equal accuracy is required throughout, several characteristics of a good network should be pointed out. The areas of the nodes should be about equal. The conductances throughout also should all be about the same. This then keeps the ratio of conductance to capacitance from being too large at any one point. The diagonal elements in the Y/A matrix are about the same size, which keeps the minimum norm low, and thus a severe stability restriction does not result. The requirement of equal areas and equal branch lengths also dictates that the network be very regular in the interior. That is, the interior nodes should approach or be the rectangular node D or the hexagonal node N.

However, a network that does not meet the requirements for equal area, equal conductance, and equal ratios y_{ij}/A_i is the trapezoidal network of a radial network of nodes bounded by arcs and radii as shown in Figure V-7. These networks are useful for many problems in radial symmetry. In this case MacNeal's trapezoids give an approximation to a direct discretization of the Laplacian operator written in the cylindrical coordinate system. The network is thus distorted based on a relationship with the boundary which is conveniently represented in

the cylindrical coordinate system. Further with this network the nodal heat capacity A_i goes to the differential volume element dV in cylindrical coordinates as the network is refined. Thus, because this makes the several finite summations for the difference solution more like the integrations for the continuous solution, it might be expected that this type of a network would have eigenvectors c_j, eigenvalues λ_j, and initial vector g that are closer to those of the continuous solution for many problems than those obtainable when a rectangular mesh is used in the interior of the circle.

Although for a problem in cylindrical symmetry a convenient orthogonal curvilinear system based on the boundary is known, for problems with a general curved boundary the distortions required for a curvilinear network in the interior would have to be estimated from the boundary geometry. Also, because the isosceles trapezoid network shape is the most general quadrilateral allowed by MacNeal's rules, networks for geometries other than cylindrical would have to be based on a distortion of a network of equilateral triangles. It would be hoped that a series expansion based on the curvilinear coordinates (not Cartesian) would show that such nodes give a high-order approximation to the Laplacian in that coordinate system. This expansion probably could not be carried out.

Further, more than one orthogonal curvilinear coordinate system can be used to describe the boundary. Thus, rather than use an

obvious coordinate system, based only on the geometry of the boundary,

one might select a network distorted according to an orthogonal curvi-

linear system that would follow or be parallel to the streamlines and

iso-potential lines.   This would give a very fine network in regions of

high gradients, as desired.   However, in a transient problem these

lines obviously can be functions of time, and only an average grid

could be used.   For problems with sufficient symmetry so that the

streamlines are not a function of time it might be possible, in principle,

to eliminate a space dimension, as the use of cylindrical coordinates

does for some problems; however, it is highly doubtful that one can

take advantage of this for most problems with irregular boundaries.

Thus, for most problems, if a distorted network is to be used, it is

probably simplest to use a distortion based on the curvilinear coordinate

system most convenient for the geometry of the boundary.

Consequently, there are two types of networks which use the

best nodes and can give good approximate solutions.   In both the

adjacent nodes follow the boundary exactly but are centered a short

distance from the boundary.   In the first network, the interior points

are located in as regular a manner as possible.   All the node shapes

approach as closely as possible either rectangles or regular hexagons.

The larger the number of points or the more regular the boundary, the

closer this approach can be made.   In the second type of network the

interior nodes are deliberately distorted in a pattern related to the

boundary or an expected temperature distribution. Examples of both types of network applied to a thick C-shaped solid are shown in Figures V-17 and V-18.

In Figure V-17 the adjacent nodes are located on straight lines that are approximately parallel to the curved boundary. This allows square nodes to be used throughout the interior of the solids; only the adjacent nodes have any irregularity, and only they require special calculation for conductances and capacitances. In addition to this advantage, the network is very simple to lay out, and the expected space discretization error is small for the nodes. Also it should be mentioned that this network shows that, by locating the adjacent points away from the boundary, and only approximately parallel to it, one can make the interior network quite regular even with a limited number of points.

The actual network shown contains 30 points. It can be made considerably coarser without destroying the description of the boundary by removing each alternate row of points or possibly only the center row. (Some small adjustments in point location would be required to maintain a good description of the boundary.) This would make the interior points rectangles, which for a problem with a constant initial temperature and a different constant boundary temperature, might give almost as good an approximate solution. This would be so because the higher gradients would occur in the horizontal direction more than in the vertical direction. Thus, the removal of the alternate rows means that

the solid can be described very well with only 18 points and a regular rectangular network of nodes can be used in the interior.

In Figure V-18 a triangular network is used on the same cross-section. This network is an attempt to distort a network of equilateral triangles (node N) for this particular geometry. This network contains 26 points which is about a 13 per cent saving in points, but each point is asymmetric and the Y/A matrix must be computed for each point.

The triangles are constructed so that they should be approximations to curvilinear triangles for an orthogonal curvilinear coordinate system convenient for the particular shape; and it would be hoped that a series expansion for the space discretization errors in these curvilinear coordinates would show that the error should be small. In general the distortion of the hexagonal nodes in the central section is what would be expected for the particular solid. In the region inside of the "prongs" of the thick C-shape, the geometry indicates that the nodes should be very small, much as the nodes become small at the center of a circle. Since the network is to be coarse, these nodes were combined to make all the nodes about equal in size. Further, the specific network used does not appear to describe the "prongs" as satisfactorily as does the rectangular network in Figure V-17.

Consequently, as the series expansions in the curvilinear coordinates cannot be readily found, there is no assurance that this network can give better or even equivalent results to a rectangular

network. Moreover, in addition to requiring a special calculation for each node to find the conductances and capacitances, this network is not as easily constructed as the rectangular network. Such a construction involves several trial and error network constructions until the location looks satisfactory, and the restrictions are satisfied. Thus, practical considerations of laying out the network and individual calculations for each point limit the use of nodes which are distorted in relationship to a curvilinear coordinate system to shapes where the convenient curvilinear coordinates are well known. Any improvement in accuracy using such an approximation could be determined by comparing, for the circular cross-section, a continuous solution with approximations using a direct discretization of the Laplacian operator in cylindrical coordinate systems with nodes bounded by arcs and radii, MacNeal trapezoids, a square network, and a network of equilateral triangles. This has not been done.

Other Rules. In addition to the discussion above about the type of node and the general network, several other points should be made concerning location of the points.

In regions where very accurate results are desired, or where the second- and higher-order derivatives are large, a small rectangular network or a network of equilateral triangles should be used. This is true even in the distorted network, as, when these nodes are refined, they tend to become rectangular. This finer mesh should also extend

away from the region of interest far enough so that any errors in the

nodes where the network size is changed, and beyond, should not affect

the solution at the particular nodes of interest. Since nodes used to

change the network size often have zero-order terms in their expan-

sions, they should be located in a region of low second derivatives

if possible. If not too many nodes are required in changing the mesh

size, equations V-72 to V-76 might be solved for each of the nodes to

improve the accuracy. The space discretization error of any node

much larger than the other nodes should be investigated, even though

it might be some distance from any region of interest. This is true

because the discretization error for this node is weighted so much

more, and can cause errors in the solution for nodes with small dis-

cretization error located some distance away.

A converse of the above rule is that, in regions where very

accurate approximations are not needed, and where the space deriv-

atives are small, a coarse network can be used. Of course, both this

region and that where the network size is changed should not be close

to nodes where high accuracy is required. An example of such a

region, where a coarse network can be safely used, is the region in the

center of a circle when the conditions of the problem are such that the

derivatives with respect to the angle parameter are small. In this

case relatively large square nodes could be safely used without affecting

the accuracy of the solution at the surface.

A corollary of the above remarks is that, for problems where the temperature differences are larger in one direction than in the perpendicular direction, a rectangular node oriented with its short dimension in the direction of the larger gradient is appropriate. This gives equivalently a small discretization error for each node without using a square node with a short dimension in both directions. Thus, the rule about having equidistant nodes can be modified under the above conditions to mean that the temperature difference between each neighboring node and the ith node should be kept constant. This rule is primarily useful in a solid with one dimension longer than the other, with constant initial temperature, and constant surrounding temperatures.

As mentioned previously, the nodes should be located so that the ratio of conductances to areas does not vary widely. Although this rule is secondary to the above comments about different-sized networks, it is of practical importance not to have one very small node with large conductances. The row or column sum associated with such a node very probably determines the minimum norm as a large number, which gives more restrictive stability and non-oscillatory criteria. Moreover, by keeping the elements of the Y/A matrix relatively in scale the effects of round-off error are somewhat reduced.

A practical application of this rule of having approximately equal ratios of conductance to capacitance is that it indicates for a composite

solid that relatively larger nodes should be used in parts of the solid where the thermal conductivity is very high, or the volumetric heat capacity low. In the extreme it helps one recognize when nodes should be combined. Further, if even the use of a large node still results in high conductance to capacitance ratio, the heat capacity of that region can be neglected. These approximations are justified by physical reasons in the Longwell report (9); however, the above rules tell us when these approximations are satisfactory.

It should be pointed out that if the transients are important in regions of high thermal conductivity, the large conductance to capacitance ratios should be used. Then a small time increment must be used not only because of stability considerations, but primarily because the temperature in such a region changes so rapidly that unless a small time increment is used the transients in that region cannot be observed. This indicates that there is no justification for including the heat capacity for such nodes, and then using the inaccurate weighting γ of 1 to allow use of a large time increment.

3.   <u>Summary--Location of Nodes.</u>

The main rule for the location of nodes where a relatively coarse network is to be used, and where the limiting number of points is known, is, for adjacent nodes:

The adjacent nodes should not be placed on the boundary, but should be located on a line approximately parallel to the surface about

half a branch length inside the surface. The solid surface forms one of the boundaries for the node . This applies both to external boundaries in contact with a fluid with a heat-transfer coefficient of 0 to infinity, inclusive, and to interfacial boundaries of a composite solid. The advantages of this type of adjacent node used to describe the boundary, over nodes located on the surface, are:

(1) This type of adjacent node can be used for all values of heat-transfer coefficients, without neglecting any heat capacity of the solid and, more importantly, without giving a severe stability restriction.

(2) An equation can be derived that shows that this type of adjacent node gives a direct discretization of the continuous boundary conditions.

(3) This somewhat flexible location of the adjacent nodes allows the internal network to be more regular, and thus it can approach more closely or be a rectangular network or a network of equilateral triangles.

The main rule for the interior nodes is:

The interior nodes should be located so that the interior network is as regular as possible. That is, each node should be as close to either the rectangular node D or the hexagonal node N, as allowed by the number of points and the boundary. The only exception to the above rule is that, if the boundary can be described in a well known curvilinear coordinate system, the nodes can be distorted as dictated by the

Laplacian operator written in those coordinates. The advantages of a regular internal network are:

(1) There are no zero-order error terms and the total discretization error should be small.

(2) The network can be relatively easily constructed, and the conductances and capacities easily found.

Two other subsidiary rules for locating the nodes are, first, a finer network of more regular nodes should be used in regions of high gradients or in regions of special interest. The corollary to this rule is that a smaller branch length should be used in directions with the largest temperature changes. Second, the ratio of conductance to capacitance should be kept about constant; nodes which have high ratios can be combined, and, if necessary, their heat capacity can be neglected.

The actual location of the adjacent nodes also follows the same general rules as indicated above for the interior points. Indeed, in actually constructing a network, obviously both the interior and adjacent nodes must be laid out on the basis of the above rules, and taking into consideration the interrelationship of their positions.

(H) SUMMARY AND CONCLUSIONS

A study has been made of the accuracy of approximate solutions for transient temperature distributions in irregular solids based on an asymmetric network of points. In this investigation the relationship between the error in the approximate solution and the discretization error, caused by replacing the continuous operators with differences, was derived as the solution of the difference equation for the propagation of the error. The discretization error caused by both the time and space differencing was studied using series expansions. The validity and usefulness of these relationships were shown by explaining the errors in numerical results for both a transient and a steady-state problem, with only a superficial knowledge of the derivatives. The important conclusions about the effects of asymmetry on the discretization error and the rules for locating the nodes and selecting the time differencing parameters are summarized below.

The series expansion based on Cartesian coordinates for the discretization error associated with the space differencing for a general asymmetric node is different from those for regular rectangular or equilateral hexagonal nodes, in that terms of lower order occur in the series for the asymmetric nodes. That is, the expansion for an asymmetric node usually contains a zero-order error term that depends only on the shape of the node and the second space derivatives, and

does not depend upon the size of the node. This is in contrast to the expansion for regular nodes mentioned above, which has as its first term in the series a second-order term that is proportional to the area of the node and the fourth space derivatives. Consequently, an approximation based on a network containing asymmetric nodes is not consistent in the Richtmyer sense, and the approximate solution cannot be made arbitrarily accurate by the addition of more points and using smaller time increments, if each succeeding network contains asymmetric nodes geometrically similar to those in the original network. However, the consistency condition can be satisfied as the network of nodes can be made regular by changing the shape of the asymmetric nodes during the refinement. Thus, the consistency condition has practical significance only for very fine networks, and it means that when a great many points can be used, they should be located in a regular network to take advantage of the small discretization error of small regular nodes. This is also dictated by practical considerations, first, that the boundaries of even an irregular solid can be followed closely with a fine regular network, and second, that the conductances and capacities are very easily determined for such networks.

However, for a relatively coarse network the size of the discretization error is important, and not how the error changes with the size of the node. Thus, the zero-order terms in the expansion have no special significance. In these cases the guide line summarized in a previous section (G-3) should be used.

Briefly, these rules are: (1) The adjacent nodes should be located not on the boundary but on a line approximately parallel to the boundary, about a half branch length from the boundary. One boundary of the nodal area coincides with the solid surface. The reasons for this are that a less severe stability restriction results, that the interior nodes can be made more regular with the same number of points, and that higher accuracy is expected because there is a better approximation to the continuous boundary equation. The spacing and location of the adjacent nodes also should follow the next several rules for the interior nodes and should allow the interior nodes to follow them.

(2) The interior network should be made as regular as possible with the nodes having as small a deviation as possible from regular rectangles or regular hexagons; any distortions should probably have a relationship to the boundary or to the expected streamlines for heat flow. All nodes should have about the same area associated with them and about equal conductances to their neighbors, with the following exceptions, listed as (3) and (4).

(3) If possible, the average branch length should be shorter in regions where a highly accurate solution is required or where the temperature gradients are large. A smaller branch length should be used in the direction of the largest gradients. For regions where the accuracy of the solution is not important and the gradients are small, a coarser network is satisfactory.

(4) The ratio of conductances to capacitances should be kept about constant to avoid having a severe stability restriction. This rule indicates, in the absence of other considerations, when nodes should be combined or when the heat capacity of a node should be neglected, and is particularly useful for composite solids of widely different thermal properties.

The selection of the time differencing parameters $\Delta\tau$ and γ for a fixed network of points is based on the stability or non-oscillatory criteria. The accuracy requirements for most problems are probably satisfied if the weighting factor γ is equal to or less than $\frac{1}{2}$. In section F-2 a procedure was shown to allow the selection of differencing parameters that would keep the calculations close to a minimum and that would give negligible oscillations. However, the numerical transient solution indicates that the continuous damping factors cannot always be bracketed by changing the time increment and the weighting factor γ, but that the inaccuracy caused by using high weighting factors is more severe for an asymmetric network than for regular networks.

Consequently, for many solids with curved or irregular boundaries, approximate solutions of adequate engineering accuracy can be obtained using relatively coarse networks of less than 30 points. This can be done by locating the points according to the above rules by following the boundary exactly and tolerating, but minimizing, any required asymmetry in the interior.

(I) SUGGESTIONS FOR FUTURE WORK

Of the many possible further investigations of approximate solutions to the diffusion equation, the following two projects show promise of giving results of important practical significance.

First, a valid expression or expansion should be developed for the discretization error for adjacent nodes with a heat-transfer co-efficient conductance to a fluid. This would allow a firm conclusion to be made about any improvement in accuracy that occurs when these adjacent nodes are located away from the boundaries. Preliminary attempts to use a Taylor series to find such an expansion have not been successful even for one-dimensional problems, probably because the difference equation was not compared to a proper combination of the boundary-condition equation and differential equation. However, future studies based on the Taylor expansion or other method should give a useful expression for this error.

Second, a relation should be developed between the error propagation analysis, used in this chapter for the asymmetric network, and the error analysis based on the complete difference solution, used in Chapter IV for regular one-dimensional networks. This would involve setting the error as given in equations V-13, V-19, or V-22 equal to the error given in equation IV-209, or other appropriate equation in Chapter IV. Such a study should allow conclusions to be made about

how the discretization error affects the error in each part of the differ-
ence solution. That is, one might be able to make precise conclusions
about how the discretization error affects the error in the particular
solution, damping factors, eigenvectors, and initial vector of the
analytic expression of the difference solution. This would then allow
the conclusions from the series expansions for the discretization error
to be applied quantitatively to the error in these parts of the solutions.
Since the discretization error expansions are more easily obtained
than are the complete difference and continuous solutions for very
general problems, this would allow a precise quantitative error analysis
for very complicated problems based only on the discretization error.

Three other suggestions that are of somewhat less importance
are:

(1) The series expansions in Cartesian coordinates for the
space discretization errors for several other node shapes should be
derived. Among the node shapes that should be studied are (a) a node
associated with an equilateral pentagonal area. The node is surrounded
by five neighboring nodes, each equidistant from the node and from each
other. (b) A node associated with an equilateral heptagonal area, sur-
rounded by seven neighboring nodes, each equidistant from the node
and from each other. Both of these nodes should have sufficient sym-
metry to give a good approximation of the Laplacian operator. Although

a network cannot be constructed merely from one of these two types

of nodes, they might be useful in other triangular networks.

Another type of node that should be further studied is the

hexagonal node. A sequence of irregular hexagons can be studied,

like the sequence of irregular quadrilateral nodes shown on Table V-9,

nodes C to I, which can be arranged to progress from a square to

trapezoidal nodes.

(2) An investigation should be made of the elimination of the

zero-order error terms in the space discretization error expansions

by solving a system of equations. Equations V-72 to V-76, when solved

for the ith node, give a corresponding row in the Y/A matrix. Equa-

tions V-77 to V-80, when solved, would give the set of lengths of p'_{ij}

for the ith node that could be used to compute the elements in the ith

row of the Y/A matrix. The specific studies required to make this

into a useful technique for the solution of the diffusion equation are

mentioned in section E-3. The results of such a study might give

weightings to use to eliminate the zero-order error term from the

expansion for irregular nodes used to change the network branch

length. Further, it would be hoped that a set of geometric conditions

of a node and its neighbors would result under which satisfactory solu-

tions could be found to these equations, so that the zero-order terms

could be eliminated from irregular interior nodes close to the

boundaries.

(3) A study should be made of the distortions of both the rectangular network and the network of equilateral triangles according to a curvilinear coordinate system based on either the boundary or an expected temperature distribution. The first part of such a study should be to determine if any improvement in accuracy occurs when such a curvilinear, or approximation to a curvilinear, network is used. This could be done by comparing the numerical results for the several possible networks for problems in circular symmetry with the continuous solution. If an analytic solution can be found for the one-dimensional partial difference equation of diffusion in cylindrical radial coordinates with z-transforms some analytic comparisons would be possible. If, the cylindrical coordinate network or MacNeal's approximation to this network does give significantly more accurate approximations when using the same number of points, then the rules for distorting both rectangular networks and networks of equilateral triangles for a general curved boundary or expected temperature distribution must be found so that such a distorted network would give a good approximation for a particular geometric boundary. This study could then result in finding a set of rules for locating temperature points in an asymmetric fashion throughout the solid in such a way that a regular mesh might require more points to give the same accuracy.

Table V-1

CONDUCTANCE MATRIX (Y) AND INVERSE CONDUCTANCE MATRIX (Y⁻¹)
First Row: Elements in Y⁻¹ Matrix; Second Row: Elements in Y Matrix
Transient Problem, Chapter III

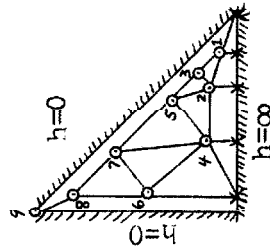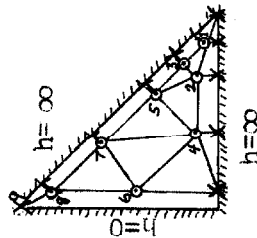|	1	2	3	4	5	6	7	8	9
1	-0.24804 -4.332	-0.05029 0.1703	-0.08799 0.750	-0.01096 0	-0.03693 0	-0.01435 0	-0.02073 0	-0.01798 0	-0.01800 0
2	-0.05029 0.1703	-0.29282 -5.653	-0.22402 2.500	-0.04860 0.3333	-0.14142 0.500	-0.05726 0	-0.08127 0	-0.07093 0	-0.07098 0
3	-0.08799 0.75	-0.22402 2.50	-0.45738 -3.755	-0.05229 0	-0.18117 0.5046	-0.06988 0	-0.10126 0	-0.08782 0	-0.08776 0
4	-0.01096 0	-0.04860 0.3333	-0.05229 0	-0.22837 -5.230	-0.13203 0.8748	-0.11752 0.40	-0.12830 0.1219	-0.12368 0	-0.12368 0
5	-0.03693 0	-0.14142 0.500	-0.18117 0.5046	-0.13203 0.8748	-0.59256 -2.480	-0.21491 0	-0.32005 0.6001	-0.27497 0	-0.27497 0
6	-0.01435 0	-0.05126 0	-0.06988 0	-0.11752 0.4000	-0.21483 0	-0.83279 -2.3981	-0.61037 1.123	-0.70563 0.375	-0.70566 0
7	-0.02073 0	-0.08127 0	-0.10126 0	-0.12830 0.1219	-0.32005 0.6001	-0.61037 1.123	-0.98275 -2.345	-0.82312 0.4999	-0.82312 0
8	-0.01798 0	-0.07098 0	-0.08782 0	-0.12368 0	-0.27497 0	-0.70563 0.375	-0.82312 0.4999	-1.91569 -1.2909	-1.91569 0.416
9	-0.01800 0	-0.07098 0	-0.08782 0	-0.12368 0	-0.27497 0	-0.70566 0.375	-0.82312 -1.91569	-1.91569 0.416	-4.31943 -0.416
Column Sums	-0.50527	-1.03164	-1.34963	-0.96543	-2.16898	-3.32837	-3.89097	-5.93556	-8.33929

Column Sums = Row Sums (Y⁻¹ Matrix)

h=0 h=∞ 0=4

Table V-2

CONDUCTANCE MATRIX (Y) AND INVERSE CONDUCTANCE MATRIX (Y⁻¹)
First Row: Elements in Y⁻¹ Matrix; Second Row: Elements in Y Matrix
Steady-State Problem, Chapter V

	1	2	3	4	5	6	7	8
1	-0.16802 -6.092	-0.01767 0.170	-0.02752 0.750	-0.00181 0	-0.00379 0	-0.00051 0	-0.00042 0	-0.00008 0
2	-0.01767 0.170	-0.22212 -5.654	-0.09311 2.500	-0.01917 0.333	-0.02729 2.500	-0.00487 0	-0.00334 0	-0.00068 0
3	-0.02752 0.75	-0.09311 2.500	-0.20238 -6.255	-0.01034 0	-0.02459 0.505	-0.00306 0	-0.00268 0	-0.00048 0
4	-0.00181 0	-0.01917 0.333	-0.01034 0	-0.20090 -5.230	-0.03053 0.875	-0.03986 0.400	-0.01220 0.122	-0.00410 0
5	-0.00379 0	-0.02729 0.500	-0.02459 0.505	-0.03053 0.875	-0.16396 -6.480	-0.01301 0	-0.01606 0.600	-0.00251 0
6	-0.00051 0	-0.00487 0	-0.00306 0	-0.03986 0.400	-0.01301 0	-0.46560 -2.398	-0.07573 1.123	-0.04140 0.375
7	-0.00042 0	-0.00334 0	-0.00268 0	-0.01220 0.122	-0.01606 0.600	-0.07573 1.123	-0.15062 -7.345	-0.02021 0.500
8	-0.00008 0	-0.00068 0	-0.00048 0	-0.00410 0	-0.00251 0	-0.04140 0.375	-0.02021 0.500	-0.19985 -5.132
Column Sums	-0.21982	-0.38825	-0.36416	-0.30891	-0.28174	-0.64403	-0.28126	-0.26931

Column Sums = Row Sums (Y⁻¹ Matrix)

Table V-3

CONDUCTANCE MATRIX (Y) AND INVERSE CONDUCTANCE MATRIX (Y^{-1})
First Row: Elements in Y^{-1} Matrix; Second Row: Elements in Y Matrix
Shape I, see Longwell (9)

	1	2	3	4	5	6	7	8	9	10	11	12	13	14
1	-0.25311 / -6.8524	-0.17448 / 0.5103	-0.17282 / 1.0206	-0.17846 / 1.0206	-0.18624 / 1.0206	-0.18963 / 0.5103	-0.06678 / 0	-0.04174 / 0	-0.09572 / 0	-0.11006 / 0	-0.03033 / 0	-0.03928 / 0	-0.00857 / 0	-0.00358 / 0
2	-0.17448 / 0.5103	-0.74674 / -2.1333	-0.34304 / 1.270	-0.20667 / 0	-0.16757 / 0	-0.15966 / 0.353	-0.20563 / 0.353	-0.07171 / 0	-0.10480 / 0	-0.10976 / 0	-0.03493 / 0	-0.04317 / 0	-0.01143 / 0	-0.00625 / 0
3	-0.17282 / 1.0206	-0.34304 / 1.270	-0.46857 / -4.2196	-0.24941 / 1.212	-0.18506 / 0	-0.17153 / 0	-0.13747 / 0.124	-0.07721 / 0.593	-0.11691 / 0	-0.12101 / 0	-0.03787 / 0	-0.04702 / 0	-0.01148 / 0	-0.00567 / 0
4	-0.17846 / 1.0206	-0.20667 / 0	-0.24941 / 1.212	-0.45644 / -4.1626	-0.27251 / 1.212	-0.23295 / 0	-0.09364 / 0	-0.07263 / 0.359	-0.16478 / 0.359	-0.16938 / 0	-0.05059 / 0	-0.06382 / 0	-0.01394 / 0	-0.00579 / 0
5	-0.18624 / 1.0206	-0.16757 / 0	-0.18506 / 0	-0.27251 / 1.212	-0.51389 / -4.2196	-0.39035 / 1.270	-0.07767 / 0	-0.06419 / 0	-0.20647 / 0.593	-0.24093 / 0.124	-0.06381 / 0	-0.08382 / 0	-0.01707 / 0	-0.00624 / 0
6	-0.18963 / 0.5103	-0.15966 / 0.353	-0.17153 / 0	-0.23295 / 0	-0.39035 / 1.270	-0.79705 / -2.1333	-0.07361 / 0	-0.06077 / 0	-0.20424 / 0	-0.30547 / 0.353	-0.06785 / 0	-0.09499 / 0	-0.01865 / 0	-0.00640 / 0
7	-0.06678 / 0	-0.20563 / 0.353	-0.13747 / 0.124	-0.09364 / 0	-0.07767 / 0	-0.07361 / 0	-0.65158 / -1.807	-0.09522 / 0.862	-0.07431 / 0	-0.06887 / 0	-0.03101 / 0	-0.03493 / 0	-0.01541 / 0	-0.01218 / 0.468
8	-0.04174 / 0	-0.07171 / 0	-0.07721 / 0.593	-0.07265 / 0.359	-0.06419 / 0	-0.06077 / 0	-0.09522 / 0.862	-0.15565 / -3.813	-0.09041 / 1.145	-0.07600 / 0	-0.03256 / 0.097	-0.03680 / 0	-0.01074 / 0	-0.00640 / 0.757
9	-0.09572 / 0	-0.10480 / 0	-0.11691 / 0	-0.16478 / 0.359	-0.20647 / 0.593	-0.20424 / 0	-0.07431 / 0	-0.09041 / 1.145	-0.45638 / -3.941	-0.35310 / 1.236	-0.12454 / 0.556	-0.14983 / 0.052	-0.03014 / 0	-0.01039 / 0
10	-0.11006 / 0	-0.10976 / 0	-0.12101 / 0	-0.16938 / 0	-0.24093 / 0.124	-0.30547 / 0.353	-0.06887 / 0	-0.07600 / 0	-0.35310 / 1.236	-0.82014 / -1.993	-0.13665 / 0	-0.21569 / 0.280	-0.03893 / 0	-0.01107 / 0
11	-0.03033 / 0	-0.03493 / 0	-0.03787 / 0	-0.05059 / 0	-0.06381 / 0	-0.06785 / 0	-0.03101 / 0	-0.03256 / 0.097	-0.12454 / 0.556	-0.13665 / 0	-0.38229 / -4.266	-0.30909 / 1.650	-0.06718 / 0.058	-0.02338 / 1.905
12	-0.03928 / 0	-0.04317 / 0	-0.04702 / 0	-0.06382 / 0	-0.08382 / 0	-0.09499 / 0	-0.03493 / 0	-0.03680 / 0	-0.14983 / 0.052	-0.21569 / 0.280	-0.30909 / 1.650	-0.71702 / -2.242	-0.11297 / 0.260	-0.02208 / 0
13	-0.00857 / 0	-0.01143 / 0	-0.01148 / 0	-0.01394 / 0	-0.01707 / 0	-0.01865 / 0	-0.01541 / 0	-0.01074 / 0	-0.03014 / 0	-0.03893 / 0	-0.06718 / 0.058	-0.11297 / 0.260	-0.49997 / -2.171	-0.02804 / 1.853
14	-0.00358 / 0	-0.00625 / 0	-0.00567 / 0	-0.00579 / 0	-0.00624 / 0	-0.00640 / 0	-0.01218 / 0.468	-0.00640 / 0.757	-0.01039 / 0	-0.01107 / 0	-0.02338 / 1.905	-0.02208 / 0	-0.02804 / 1.853	-0.02902 / -38.150
Column Sums	-1.55090	-2.38783	-2.14509	-2.23103	-2.47581	-2.77314	-1.63831	-0.89204	-2.18203	-2.77704	-1.39207	-1.97052	-0.88443	-0.17648

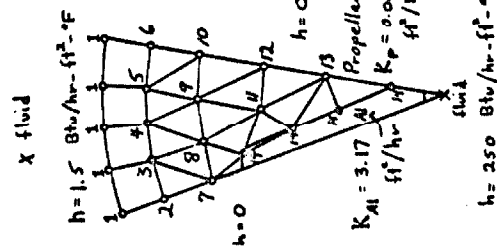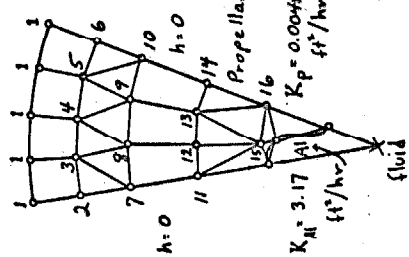Column Sums = Row Sums $(Y^{-1}$ Matrix$)$

Table V-4

CONDUCTANCE MATRIX (Y) AND INVERSE CONDUCTANCE MATRIX (Y⁻¹)

First Row: Elements in Y⁻¹ Matrix; Second Row: Elements in Y Matrix

Shape II, see Longwell (9)

Diagram labels:
- X fluid
- $h = 1.5$ Btu/hr·ft²·°F
- h_2O
- Propellant
- $K_P = 0.00480$ ft²/hr
- $K_{Al} = 3.17$ All ft²/hr
- fluid
- $h = 250$ Btu/hr·ft²·°F
- (Heat capacity of Aluminum neglected)

|	1	2	3	4	5	6	7	8	9	10	11	12	13	14	15	16
1	-0.2834 / -6.8554	-0.2455 / 0.5103	-0.2440 / 1.0206	-0.2389 / 1.0206	-0.2249 / 1.0206	-0.1867 / 0.5103	-0.1960 / 0	-0.1937 / 0	-0.1871 / 0	-0.1792 / 0	-0.1233 / 0	-0.1219 / 0	-0.1186 / 0	-0.1157 / 0	-0.0120 / 0	-0.0016 / 0
2	-0.2455 / 0.5103	-0.8930 / -2.1333	-0.4896 / 1.270	-0.3379 / 0	-0.2691 / 0	-0.2118 / 0	-0.4475 / 0.353	-0.3649 / 0	-0.2932 / 0	-0.2632 / 0	-0.2350 / 0	-0.2232 / 0	-0.2050 / 0	-0.1948 / 0	-0.0222 / 0	-0.0027 / 0
3	-0.2440 / 1.0206	-0.4896 / 1.270	-0.6166 / -4.2196	-0.3812 / 1.212	-0.2860 / 0	-0.2211 / 0	-0.3878 / 0.124	-0.3727 / 0.593	-0.3056 / 0	-0.2739 / 0	-0.2271 / 0	-0.2213 / 0	-0.2065 / 0	-0.1972 / 0	-0.0218 / 0	-0.0028 / 0
4	-0.2389 / 1.0206	-0.3379 / 0	-0.3812 / 1.212	-0.5713 / -4.1626	-0.3548 / 1.212	-0.2568 / 0	-0.3419 / 0.359	-0.3419 / 0.359	-0.3326 / 0.359	-0.3018 / 0	-0.2129 / 0	-0.2122 / 0	-0.2068 / 0	-0.2006 / 0	-0.0209 / 0	-0.0028 / 0
5	-0.2249 / 1.0206	-0.2691 / 0	-0.2860 / 0	-0.3548 / 1.212	-0.5575 / -4.2196	-0.3558 / 1.270	-0.2721 / 0	-0.2899 / 0	-0.3365 / 0.593	-0.3338 / 0.124	-0.1924 / 0	-0.1945 / 0	-0.1983 / 0	-0.1974 / 0	-0.0192 / 0	-0.0026 / 0
6	-0.1867 / 0.5103	-0.2118 / 0	-0.2211 / 0	-0.2568 / 0	-0.3558 / 1.270	-0.6287 / -2.6436	-0.2148 / 0	-0.2285 / 0	-0.2712 / 0	-0.3251 / 0.353	-0.1563 / 0	-0.1588 / 0	-0.1647 / 0	-0.1694 / 0	-0.0157 / 0	-0.0022 / 0
7	-0.1960 / 0	-0.4475 / 0.353	-0.3878 / 0.124	-0.3419 / 0.359	-0.2721 / 0	-0.2148 / 0	-1.0260 / -1.997	-0.5843 / 1.235	-0.4018 / 0	-0.3462 / 0	-0.4250 / 0.285	-0.3762 / 0	-0.3245 / 0	-0.3044 / 0	-0.0375 / 0	-0.0044 / 0
8	-0.1937 / 0	-0.3649 / 0	-0.3727 / 0.593	-0.3419 / 0.359	-0.2899 / 0	-0.2285 / 0	-0.5843 / 1.235	-0.7162 / -3.947	-0.4604 / 1.19	-0.3879 / 0	-0.3768 / 0	-0.3746 / 0.57	-0.3355 / 0	-0.3139 / 0	-0.0366 / 0	-0.0045 / 0
9	-0.1871 / 0	-0.2932 / 0	-0.3056 / 0	-0.3326 / 0.359	-0.3365 / 0.593	-0.2712 / 0	-0.4018 / 0	-0.4604 / 1.19	-0.6969 / -3.947	-0.5499 / 1.235	-0.3245 / 0	-0.3353 / 0	-0.3588 / 0.57	-0.3511 / 0	-0.0309 / 0	-0.0049 / 0
10	-0.1792 / 0	-0.2632 / 0	-0.2739 / 0	-0.3018 / 0	-0.3338 / 0.124	-0.3251 / 0.353	-0.3462 / 0	-0.3879 / 0	-0.5499 / 1.235	-0.9748 / -1.997	-0.2998 / 0	-0.3129 / 0	-0.3485 / 0	-0.3909 / 0.285	-0.0309 / 0	-0.0049 / 0
11	-0.1233 / 0	-0.2350 / 0	-0.2271 / 0	-0.2129 / 0	-0.1924 / 0	-0.1563 / 0	-0.4250 / 0.285	-0.3768 / 0	-0.3245 / 0	-0.2998 / 0	-0.9553 / -2.694	-0.5405 / 2.25	-0.4765 / 0	-0.4174 / 0	-0.0703 / 0.159	-0.0066 / 0
12	-0.1219 / 0	-0.2232 / 0	-0.2213 / 0	-0.2122 / 0	-0.1945 / 0	-0.1588 / 0	-0.3762 / 0	-0.3746 / 0.57	-0.3353 / 0	-0.3129 / 0	-0.6405 / 2.25	-0.7146 / -5.401	-0.5257 / 2.25	-0.4585 / 0	-0.0663 / 0.331	-0.0070 / 0
13	-0.1186 / 0	-0.2050 / 0	-0.2065 / 0	-0.2068 / 0	-0.1983 / 0	-0.1647 / 0	-0.3245 / 0	-0.3355 / 0	-0.3588 / 0.57	-0.3485 / 0	-0.4765 / 0	-0.5257 / 2.25	-0.6928 / -5.194	-0.5968 / 2.02	-0.0523 / 0.05	-0.0095 / 0.304
14	-0.1157 / 0	-0.1948 / 0	-0.1972 / 0	-0.2006 / 0	-0.1974 / 0	-0.1694 / 0	-0.3004 / 0	-0.3139 / 0	-0.3511 / 0	-0.3909 / 0.285	-0.4174 / 0	-0.4585 / 0	-0.5968 / -5.194	-0.9224 / -2.514	-0.0459 / 0	-0.0092 / 0.209
15	-0.0120 / 0	-0.0222 / 0	-0.0218 / 0	-0.0209 / 0	-0.0192 / 0	-0.0157 / 0	-0.0379 / 0	-0.0366 / 0	-0.0330 / 0	-0.0309 / 0	-0.0703 / 0.159	-0.0663 / 0.331	-0.0523 / 0.05	-0.0459 / 0	-0.1855 / -5.6088	-0.0047 / 1.0219
16	-0.0016 / 0	-0.0027 / 0	-0.0028 / 0	-0.0028 / 0	-0.0026 / 0	-0.0022 / 0	-0.0044 / 0	-0.0045 / 0	-0.0047 / 0	-0.0048 / 0	-0.0066 / 0	-0.0070 / 0	-0.0085 / 0.304	-0.0092 / 0.209	-0.0047 / 1.0219	-0.0220 / -5.9019
Column Sums	-2.6725	-4.6986	-4.4552	-4.2986	-4.0848	-3.5676	-5.6701	-5.3823	-5.2426	-5.3236	-5.1397	-4.9435	-4.8198	-4.8816	-5.6752	-0.0911

Column Sums = Row Sums (Y⁻¹ Matrix)

Table V-5

CONDUCTANCE MATRIX (Y) AND INVERSE CONDUCTANCE MATRIX (Y^{-1})

First Row: Elements in Y^{-1} Matrix; Second Row: Elements in Y Matrix

Square Grid — Specified Surface Temperature

	1	2	3	4	5	6	7	8	9
1	-0.29911 / -4.0	-0.09821 / 1.0	-0.03125 / 0	-0.09821 / 1.0	-0.05250 / 0	-0.02679 / 0	-0.03125 / 0	-0.02679 / 0	-0.01339 / 0
2	-0.09821 / 1.0	-0.33036 / -4.0	-0.09821 / 1.0	-0.05250 / 0	-0.12500 / 1.0	-0.06250 / 0	-0.02679 / 0	-0.04464 / 0	-0.02679 / 0
3	-0.03125 / 0	-0.09821 / 1.0	-0.29911 / -4.0	-0.02679 / 0	-0.05250 / 0	-0.09821 / 1.0	-0.01339 / 0	-0.02679 / 0	-0.03125 / 0
4	-0.09821 / 1.0	-0.06250 / 0	-0.02679 / 0	-0.33036 / -4.0	-0.12500 / 1.0	-0.04464 / 0	-0.09821 / 1.0	-0.06250 / 0	-0.02679 / 0
5	-0.06250 / 0	-0.12500 / 1.0	-0.06250 / 0	-0.12500 / 1.0	-0.37500 / -4.0	-0.12500 / 1.0	-0.06250 / 0	-0.12500 / 1.0	-0.06250 / 0
6	-0.02679 / 0	-0.06250 / 0	-0.09821 / 1.0	-0.04464 / 0	-0.12500 / 1.0	-0.33036 / -4.0	-0.02679 / 0	-0.06250 / 0	-0.09821 / 1.0
7	-0.03125 / 0	-0.02679 / 0	-0.01339 / 0	-0.09821 / 1.0	-0.06250 / 0	-0.02679 / 0	-0.29911 / -4.0	-0.09821 / 1.0	-0.03125 / 0
8	-0.02679 / 0	-0.04464 / 0	-0.02679 / 0	-0.06250 / 0	-0.12500 / 1.0	-0.06250 / 0	-0.09821 / 1.0	-0.33036 / -4.0	-0.09821 / 1.0
9	-0.01339 / 0	-0.02679 / 0	-0.03125 / 0	-0.02679 / 0	-0.06250 / 0	-0.09821 / 1.0	-0.03125 / 0	-0.09821 / 1.0	-0.29911 / -4.0
Column Sums	-0.68750	-0.87500	-0.68750	-0.87500	-1.12500	-0.87500	-0.68750	-0.87500	-0.68750

Column Sums = Row Sums (Y^{-1} Matrix)

$\Delta\xi = \Delta\eta$
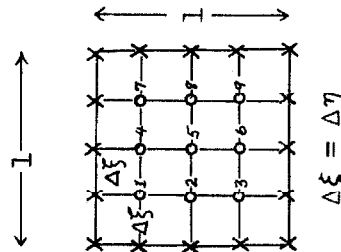
Table V-6

CONDUCTANCE MATRIX (Y) AND INVERSE CONDUCTANCE MATRIX (Y⁻¹)

First Row: Elements in Y^{-1} Matrix; Second Row: Elements in Y Matrix

Regular Rectangular Grid – Specified Surface Temperature

	1	2	3	4	5	6	7	8	9
1	-0.25504 -5.0	-0.04191 0.50	-0.00798 0	-0.12712 2.0	-0.03902 0	-0.00947 0	-0.05300 0	-0.02150 0	-0.00594 0
2	-0.04191 0.50	-0.26302 -5.0	-0.04191 0.50	-0.03902 0	-0.13659 2.0	-0.03902 0	-0.02150 0	-0.05893 0	-0.02150 0
3	-0.00798 0	-0.04191 0.50	-0.25504 -5.0	-0.00947 0	-0.03902 0	-0.12712 2.0	-0.00594 0	-0.02150 0	-0.05300 0
4	-0.12712 2.0	-0.03902 0	-0.00947 0	-0.30803 -5.0	-0.06341 0.50	-0.01392 0	-0.12712 2.0	-0.03902 0	-0.00947 0
5	-0.03902 0	-0.13659 2.0	-0.03902 0	-0.06341 0.50	-0.32195 -5.0	-0.06341 0.50	-0.03902 0	-0.13659 2.0	-0.03902 0
6	-0.00947 0	-0.03902 0	-0.12712 2.0	-0.01392 0	-0.06341 0.50	-0.30803 -5.0	-0.00947 0	-0.03902 0	-0.12712 2.0
7	-0.05300 0	-0.02150 0	-0.00594 0	-0.12712 2.0	-0.03902 0	-0.00947 0	-0.25504 -5.0	-0.04191 0.50	-0.00798 0
8	-0.02150 0	-0.05893 0	-0.02150 0	-0.03902 0	-0.13659 2.0	-0.03902 0	-0.04191 0.50	-0.26302 -5.0	-0.04191 0.50
9	-0.00594 0	-0.02150 0	-0.05300 0	-0.00947 0	-0.03902 0	-0.12712 2.0	-0.00798 0	-0.04191 0.50	-0.25504 -5.0
Column Sums	-0.56098	-0.66341	-0.56098	-0.73659	-0.87805	-0.73659	-0.56098	-0.66341	-0.56098

Column Sums = Row Sums (Y^{-1} Matrix)

$\Delta\eta = 2\Delta\xi$
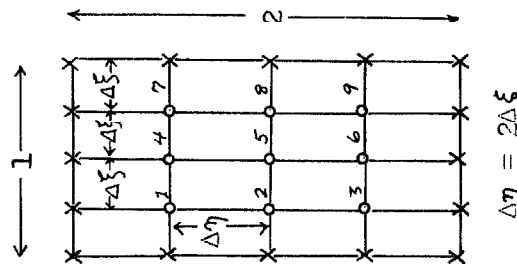
Table V-7

STEADY-STATE STUDY, SQUARE SHAPE

Continuous, Approximate Solutions, Errors, and Discretization Error

Node i	1	2	3	4	5	6	7	8
Continuous Solution, $T_{i,SS}$	0.7953	0.7947	0.6557	0.8909	0.5888	0.6900	0.5451	0.5164
Approximate Solution, $t_{i,SS}$	0.7886	0.8015	0.6626	0.8850	0.5920	0.6922	0.5445	0.5184
Error, $v_{i,SS} = T_{i,SS} - t_{i,SS}$	0.0067	-0.0068	-0.0069	0.0059	-0.0032	-0.0022	0.0006	-0.0020
Area-Weighted Discretization Error, $A_i d_{i,SS}$	-0.0468	0.0229	0.0293	-0.0369	0.0198	0.0075	-0.0084	0.0095
Discretization Error, $d_{i,SS}$	-13.69	3.952	6.350	-2.132	1.364	0.3102	-0.4373	0.6426
(2) Approximate Solution	0.7988	0.8026	0.6642	0.8851	0.5923	0.6922	0.5446	0.5184
Error	-0.0035	-0.0079	-0.0085	0.0058	-0.0035	-0.0022	0.0005	-0.0020
Area-Weighted Discretization Error	0.0136	As In (1)						
(3) Approximate Solution	0.8089	0.8037	0.6659	0.8852	0.5925	0.6923	0.5446	0.5184
Error	-0.0136	-0.0090	-0.0102	0.0057	-0.0037	0.0023	0.0005	0.0020
Area-Weighted Discretization Error	0.0740	As In (1)						

Approximate Calculation (1) Uses $t_B = T_B$

(2) Uses $t_B = T_B$ except for node at A which is used as 3/4 instead of 1/2

(3) Uses $t_B = T_B$ except for node A which is taken as 1 instead of 1/2

Table V-8

TAYLOR SERIES EXPANSION

$$(T_j - T_i)$$

$$\frac{\rho_{ij}}{\lambda_{ij}}(T_j - T_i) = \frac{\rho_{ij}}{\lambda_{ij}} \sum_{p=1}^{\infty} \frac{1}{p!}\left[\lambda_{ij}\left\{\cos\beta_{ij}\frac{\partial}{\partial\xi} + \sin\beta_{ij}\frac{\partial}{\partial\eta}\right\}\right]^p T_{i,n}$$

p	Terms
1	$\rho_{ij}\left[\cos\beta_{ij}\dfrac{\partial T_{i,n}}{\partial\xi} + \sin\beta_{ij}\dfrac{\partial T_{i,n}}{\partial\eta}\right]$
2	$\dfrac{\rho_{ij}\lambda_{ij}}{2}\left[(\cos\beta_{ij})^2\dfrac{\partial^2 T_{i,n}}{\partial\xi^2} + 2\cos\beta_{ij}\sin\beta_{ij}\dfrac{\partial^2 T_{i,n}}{\partial\xi\,\partial\eta} + (\sin\beta_{ij})^2\dfrac{\partial^2 T_{i,n}}{\partial\eta^2}\right]$
3	$\dfrac{\rho_{ij}(\lambda_{ij})^2}{6}\left[(\cos\beta_{ij})^3\dfrac{\partial^3 T_{i,n}}{\partial\xi^3} + 3(\cos\beta_{ij})^2(\sin\beta_{ij})\dfrac{\partial^3 T_{i,n}}{\partial\xi^2\partial\eta^2}\right.$ $\left. + 3(\cos\beta_{ij})(\sin\beta_{ij})^2\dfrac{\partial^3 T_{i,n}}{\partial\xi\partial\eta^2} + (\sin\beta_{ij})^3\dfrac{\partial^3 T_{i,n}}{\partial\eta^3}\right]$
4	$\dfrac{\rho_{ij}(\lambda_{ij})^3}{24}\left[(\cos\beta_{ij})^4\dfrac{\partial^4 T_{i,n}}{\partial\xi^4} + 4(\cos\beta_{ij})^3(\sin\beta_{ij})\dfrac{\partial^4 T_{i,n}}{\partial\xi^3\partial\eta} + \right.$ $+ 6(\cos\beta_{ij})^2(\sin\beta_{ij})^2\dfrac{\partial^4 T_{i,n}}{\partial\xi^2\partial\eta^2} + 4(\cos\beta_{ij})(\sin\beta_{ij})^3\dfrac{\partial^4 T_{i,n}}{\partial\xi\partial\eta^3} +$ $\left. + (\sin\beta_{ij})^4\dfrac{\partial^4 T_{i,n}}{\partial\eta^4}\right]$
⋮	⋮

Table V-9

SPACE DISCRETIZATION ERROR

Notes Pertaining to This Table:

(1) If the last term in the expansion contains a derivative of order p, the next term not shown contains a derivative of order (p+1); all terms containing p are shown.

(2) o Location of node   X Location of neighboring node

(3) Letter at origin designates node

(4) —— Conductance, length of network leg   - - - - Perpendicular Bisector, designates node shape and area

Node i	Expansion for $\sigma_{i,n} = \dfrac{1}{A_i} \displaystyle\sum_{j=1}^{N} y_{ij}(T_{j,n} - T_{i,n}) - \nabla'^2 T_{i,n}$
A	One-Dimensional Problem in Cartesian Coordinates* $$\left[\frac{\lambda_1 - \lambda_2}{3}\right]\left[\frac{\partial^3 T_{A,n}}{\partial \xi^3}\right] + \left[\frac{\lambda_1^2 - \lambda_1\lambda_2 + \lambda_2^2}{12}\right]\left[\frac{\partial^4 T_{A,n}}{\partial \xi^4}\right] + \cdots$$
B	One-Dimensional Problem in Cartesian Coordinates, Regular Network $\lambda_1 = \lambda_2$ * $$\left[\frac{(\Delta\xi)^2}{12}\right]\left[\frac{\partial^4 T_{B,n}}{\partial \xi^4}\right] + \cdots$$

* Based on Laplacian operator, one-dimensional problem

Table V-9 (Cont.)

SPACE DISCRETIZATION ERROR
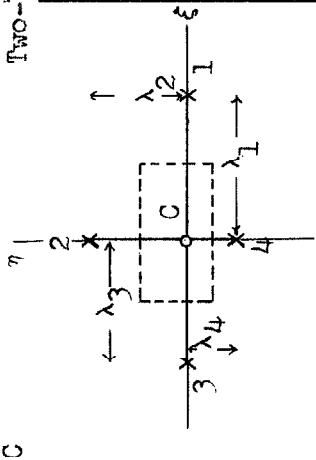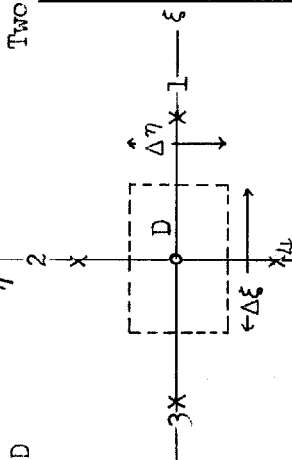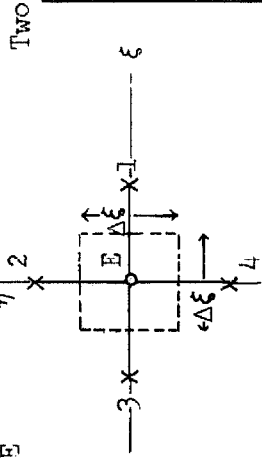
Node i	Expansion for $\sigma_{i,n}$	
C	**Two-Dimensional Irregular Rectangular Node** $$\frac{1}{3}\left[(\lambda_1-\lambda_3)\frac{\partial^3 T_{C,n}}{\partial\xi^3} + (\lambda_2-\lambda_4)\frac{\partial^3 T_{C,n}}{\partial\eta^3}\right]$$ $$+\frac{1}{12}\left[(\lambda_1^2-\lambda_1\lambda_3+\lambda_3^2)\frac{\partial^4 T_{C,n}}{\partial\xi^4} + (\lambda_2^2-\lambda_2\lambda_4+\lambda_4^2)\frac{\partial^4 T_{C,n}}{\partial\eta^4}\right]+\cdots$$	
D	**Two-Dimensional Regular Rectangular Node** $$\frac{1}{12}\left[(\Delta\xi)^2\frac{\partial^4 T_{D,n}}{\partial\xi^4} + (\Delta\eta)^2\frac{\partial^4 T_{D,n}}{\partial\eta^4}\right]+\cdots$$ $$\lambda_1=\lambda_3=\Delta\xi$$ $$\lambda_2=\lambda_4=\Delta\eta$$	
E	**Two-Dimensional Square Node** $$\lambda_1=\lambda_2=\lambda_3=\lambda_4=\Delta\xi=\Delta\eta$$ $$\frac{(\Delta\xi)^2}{12}\left[\frac{\partial^4 T_{E,n}}{\partial\xi^4} + \frac{\partial^4 T_{E,n}}{\partial\eta^4}\right]+\cdots$$	

Table V-9 (Cont.)

SPACE DISCRETIZATION ERROR
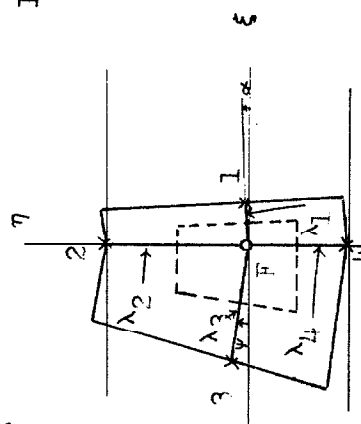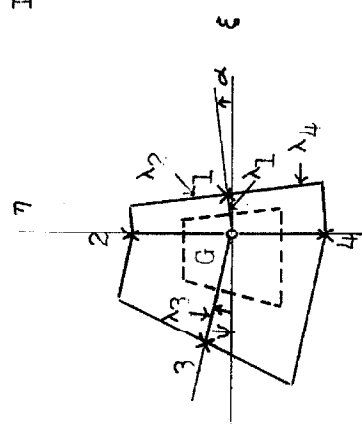
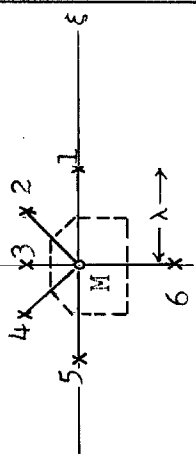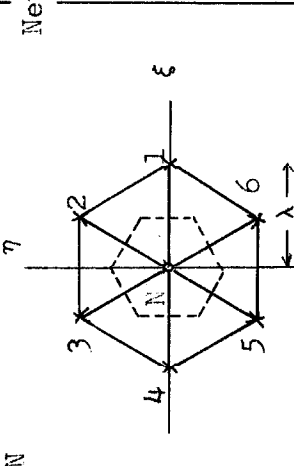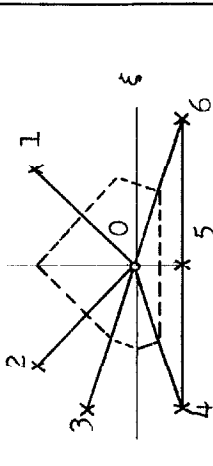| Node i	Expansion for $\sigma_{i,n}$
F	Irregular Trapezoidal Node $$\frac{(\lambda_2-\lambda_4)(\sin\alpha)\left[\sin(\alpha+\psi)\right]-2\lambda_1\left[(\cos\psi)(\sin\alpha)^3+(\cos\alpha)(\sin\psi)^3\right]}{\left[\sin(\alpha+\psi)\right]\left[2\lambda_1+(\lambda_4-\lambda_2)\sin\alpha\right]}\left[\frac{\partial^2 T_{F,n}}{\partial\xi^2}-\frac{\partial^2 T_{F,n}}{\partial\eta^2}\right]$$ $$+\left[\frac{2\lambda_1\cos\alpha\cos\psi\,\sin(\alpha-\psi)}{2\lambda_1+(\lambda_4-\lambda_2)(\sin\alpha)}\right]\frac{\partial^2 T_{F,n}}{\partial\xi\,\partial\eta}+\cdots$$
G	Irregular Trapezoidal Node $$\lambda_2=\lambda_4 \qquad \lambda_1\neq\lambda_3 \qquad \alpha\neq\psi$$ $$-\left[\frac{(\sin\alpha)^3(\cos\psi)+(\sin\psi)^3(\cos\alpha)}{\sin(\alpha+\psi)}\right]\left[\frac{\partial^2 T_{G,n}}{\partial\xi^2}-\frac{\partial^2 T_{G,n}}{\partial\eta^2}\right]+$$ $$+\left[(\cos\alpha)(\cos\psi)\sin(\alpha-\psi)\right]\left[\frac{\partial^2 T_{G,n}}{\partial\xi\,\partial\eta}\right]+\cdots$$

Table V-9 (Cont.)

SPACE DISCRETIZATION ERROR

Node i	Expansion for $\sigma_{i,n}$
H	**Irregular Trapezoidal Node** $\lambda_2 \neq \lambda_4$ $\lambda_1 = \lambda_3$ $\alpha = \psi$ $$\left[\frac{(\sin\alpha)\left[(\lambda_2-\lambda_4)-2\lambda_1\sin\alpha\right]}{(\lambda_4-\lambda_2)(\sin\alpha)+2\lambda_1} \right]\left\{ \frac{\partial^2 T_{H,n}}{\partial\xi^2} - \frac{\partial^2 T_{H,n}}{\partial\eta^2} \right\} + \cdots$$
I	**Regular Trapezoidal Node** $\lambda_2 = \lambda_4 = \Delta\rho$ $\lambda_1 = \lambda_3$ $\alpha = \psi = \Delta\theta/2$ $$(\sin\alpha)^2\left[\frac{\partial^2 T_{I,n}}{\partial\xi^2} - \frac{\partial^2 T_{I,n}}{\partial\eta^2} \right] + \lambda_1\sin\alpha(\cos\alpha)^2\frac{\partial^3 T_{I,n}}{\partial\xi^2\partial\eta}$$ $$+ \left[\frac{\sin\alpha}{3}\right]\left[\lambda_1(\sin\alpha)^2 - \frac{\lambda_2^2}{\lambda_1}\right]\frac{\partial^3 T_{I,n}}{\partial\eta^3} + \cdots$$ or $$\frac{1}{2}(\cos\Delta\theta-1)\left[\frac{\partial^2 T_{I,n}}{\partial\xi^2} - \frac{\partial^2 T_{I,n}}{\partial\eta^2}\right] + \lambda_1\left(\sin\frac{\Delta\theta}{2}\right)\left(\cos\frac{\Delta\theta}{2}\right)^2\frac{\partial^3 T_{I,n}}{\partial\xi^2\partial\eta}$$ $$+ \frac{1}{3}\left(\sin\frac{\Delta\theta}{2}\right)\left[\lambda_1\left(\sin\frac{\Delta\theta}{2}\right)^2 - \frac{(\Delta\rho)^2}{\lambda_1}\right]\frac{\partial^3 T_{I,n}}{\partial\eta^3} + \cdots$$

Table V-9 (Cont.)

SPACE DISCRETIZATION ERROR
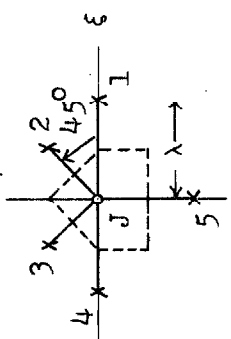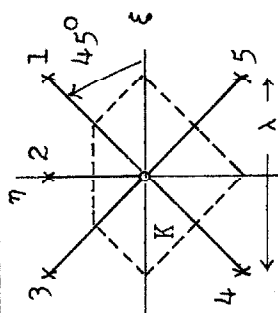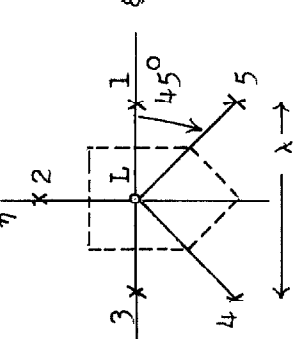
Node i	Expansion for $\sigma_{i,n}$
J	Node for Changing Network Size: MacNeal (8), Fig. 6A $$-\frac{\lambda}{6}\left[\frac{\partial^3 T_{J,n}}{\partial \eta^3} - \frac{\partial^3 T_{J,n}}{\partial \xi^2 \partial \eta}\right] + \cdots$$
K	Node for Changing Network Size: MacNeal (8), Fig. 6A $$-\frac{1}{7}\left[\frac{\partial^2 T_{K,n}}{\partial \xi^2} - \frac{\partial^2 T_{K,n}}{\partial \eta^2}\right] - \frac{\lambda}{7}\left[\frac{\partial^3 T_{K,n}}{\partial \xi^2 \partial \eta}\right] + \cdots$$
L	Node for Changing Network Size: MacNeal (8), Fig. 6A $$\frac{1}{5}\left[\frac{\partial^2 T_{L,n}}{\partial \xi^2} - \frac{\partial^2 T_{L,n}}{\partial \eta^2}\right] - \frac{\lambda}{5}\left[\frac{\partial^3 T_{L,n}}{\partial \xi^2 \partial \eta}\right] + \cdots$$

485

Table V-9 (Cont.)

SPACE DISCRETIZATION ERROR

Node i	Expansion for $\sigma_{i,n}$	
M	Node for Changing Network Size: MacNeal (8), Fig. 6B $$-\frac{1}{11}\left[\frac{\partial^2 T_{M,n}}{\partial\xi^2} - \frac{\partial^2 T_{M,n}}{\partial\eta^2}\right] + \frac{\lambda}{11}\left[\frac{\partial^3 T_{M,n}}{\partial\xi^2\partial\eta} - 2\frac{\partial^3 T_{M,n}}{\partial\eta^3}\right] + \cdots$$	
N	Network of Equilateral Triangles: Hexagonal Node $$\frac{\lambda^2}{16}\left[\frac{\partial^4 T_{N,n}}{\partial\xi^4} + 2\frac{\partial^4 T_{N,n}}{\partial\xi^2\partial\eta^2} + \frac{\partial^4 T_{N,n}}{\partial\eta^4}\right] + \cdots$$ or $$\frac{\lambda^2}{16}\left[\nabla'^4 T_{N,n}\right] + \cdots$$	
O	Node 1 in Figure III-1: Adiabatic or Symmetric Boundary about Hypotenuse $$0.070\left[\frac{\partial^2 T_{O,n}}{\partial\xi^2} - \frac{\partial^2 T_{O,n}}{\partial\eta^2}\right] - 0.019\left[\frac{\partial^2 T_{O,n}}{\partial\xi\partial\eta}\right] + \cdots$$	

Table V-9 (Cont.)

SPACE DISCRETIZATION ERROR

Node i	Expansion for $\sigma_{i,n}$
P	Node 6 in Figure III-1 $$-0.039\left[\frac{\partial^2 T_{p,n}}{\partial \xi^2} - \frac{\partial^2 T_{p,n}}{\partial \eta^2}\right] + 0.064\left[\frac{\partial^2 T_{p,n}}{\partial \xi \partial \eta}\right] + \cdots$$

Table V-10

ERRORS - TRANSIENT PROBLEM - CHAPTER III

γ	$\Delta\tau$	τ	T_1-t_1	T_2-t_2	T_3-t_3	T_4-t_4	T_5-t_5	T_6-t_6	T_7-t_7	T_8-t_8	T_9-t_9
Analog	0	0.003	0.0046	-0.0276	-0.0203	-0.1010	0.0179	0.0549	0.0111	0.0025	0.0006
0	0.0001		0.0094	-0.0235	-0.0155	-0.0975	0.0171	0.0549	0.0107	0.0025	0.0006
	0.0005		0.0249	-0.0060	0.0065	-0.0824	0.0132	0.0551	0.0093	0.0021	0.0004
	0.001		0.0668	0.0377	0.0162	-0.0612	0.0071	0.0551	0.0073	0.0016	0.0002
0.5	0.0005		0.0066	-0.0269	-0.0199	-0.1006	0.0177	0.0549	0.0111	0.0026	0.0007
	0.0015		0.0192	-0.0231	-0.0140	-0.0971	0.0154	0.0548	0.0110	0.0026	0.0007
1.0	0.0005		-0.0222	-0.0472	-0.0406	-0.1174	0.0125	0.0549	0.0128	0.0031	0.0010
Analog	0	0.006	0.0018	-0.0142	-0.0099	-0.0377	-0.0076	0.0600	0.0284	0.0108	0.0045
0	0.0001		0.0030	-0.0113	-0.0062	-0.0347	-0.0071	0.0602	0.0279	0.0106	0.0044
	0.0005		0.0073	0.0002	0.0088	-0.0224	-0.0051	0.0609	0.0261	0.0098	0.0038
	0.001		0.0104	0.0131	0.0299	-0.0061	-0.0020	0.0619	0.0236	0.0090	0.0029
0.5	0.0005		0.0020	-0.0137	-0.0094	-0.0374	-0.0078	0.0600	0.0283	0.0108	0.0046
	0.0015		0.0035	-0.0106	-0.0052	-0.0346	-0.0088	0.0600	0.0280	0.0108	0.0046
1.0	0.0005		-0.0047	-0.0280	-0.0279	-0.0521	-0.0099	0.0592	0.0304	0.0118	0.0065

Table V-10(Cont.)

ERRORS - TRANSIENT PROBLEM - CHAPTER III

γ	ΔT	T	T_1-t_1	T_2-t_2	T_3-t_3	T_4-t_4	T_5-t_5	T_6-t_6	T_7-t_7	T_8-t_8	T_9-t_9
Analog		0.01									
0	0		0.0004	-0.0057	-0.0035	0.0019	-0.0146	0.0456	0.0322	0.0256	0.0162
	0.0001		0.0009	-0.0043	-0.0016	0.0036	-0.0131	0.0459	0.0319	0.0253	0.0159
	0.0005		0.0028	0.0313	0.0056	0.0106	-0.0070	0.0471	0.0310	0.0241	0.0146
	0.001		0.0048	0.0078	0.0141	0.0191	0.0014	0.0486	0.0298	0.0225	0.0130
0.5	0.0005		0.0005	-0.0056	-0.0032	0.0021	-0.0146	0.0456	0.0321	0.0256	0.0162
	0.0015*		0.0034	0.0335	0.0089	0.0130	0.0033	0.0554	0.0407	0.0297	0.0184
	0.01		0.5778	0.2404	0.0892	0.1563	-0.0706	0.0439	0.0163	0.0238	0.0169
1.0	0.0005		-0.0021	-0.0131	-0.0129	-0.0069	-0.0215	0.0443	0.0332	0.0270	0.0177
	0.01		-0.0973	-0.1493	-0.1733	-0.1481	-0.0961	0.0241	0.0412	0.0448	0.0373
Analog		0.05									
0	0		0.0002	0.0008	0.0018	0.0079	0.0058	0.0019	0.0009	0.0086	0.0116
	0.0001		0.0003	0.0010	0.0019	0.0080	0.0061	0.0021	0.0013	0.0089	0.0119
	0.0005		-0.0001	0.0013	0.0022	0.0084	0.0071	0.0035	0.0029	0.0103	0.0132
	0.001		0.0004	0.0016	0.0027	0.0089	0.0093	0.0053	0.0050	0.0120	0.0145
0.5	0.0005		0.0002	0.0009	0.0018	0.0079	0.0058	0.0017	0.0009	0.0086	0.0115
	0.0015*		0.0002	0.0004	0.0012	0.0072	0.0042	-0.0017	-0.0033	0.0040	0.0065
	0.01		0.1509	0.0292	-0.0497	0.0087	0.0090	0.0033	0.0031	0.0031	0.0106
1.0	0.0005		0.0001	0.0005	0.0013	0.0074	0.0045	0.0001	-0.0012	0.0069	0.0101
	0.01		-0.0025	-0.0090	-0.0108	-0.0042	-0.0248	-0.0301	-0.0384	-0.0190	-0.0135

*Data for $\gamma=0.5$, $\Delta T=0.0015$ taken at increment closest to T.

Table V-10(Cont.)

ERRORS – TRANSIENT PROBLEM – CHAPTER III

γ	$\Delta\tau$	τ	T_1-t_1	T_2-t_2	T_3-t_3	T_4-t_4	T_5-t_5	T_6-t_6	T_7-t_7	T_8-t_8	T_9-t_9
Analog	0	0.10	-0.0001	-0.0004	-0.0003	0.0016	-0.0005	-0.0059	-0.0072	-0.0107	-0.0108
0	0.0001		-0.0001	-0.0004	-0.0002	0.0016	-0.0004	-0.0058	-0.0069	-0.0104	-0.0104
	0.0005		-0.0001	-0.0003	-0.0001	0.0019	0.00004	-0.0045	-0.0058	-0.0088	-0.0088
	0.001		-0.00003	-0.0001	-0.0001	0.0021	0.0006	-0.0036	-0.0045	-0.0069	-0.0068
0.5	0.0005		-0.0001	-0.0004	-0.0003	0.0016	-0.0005	-0.0060	-0.0072	-0.0107	-0.0108
	0.0015*		0.0030	-0.0002	-0.0001	0.0019	0.0001	-0.0043	-0.0060	-0.0085	-0.0089
	0.01		0.0004	-0.0085	0.0144	0.0019	-0.0004	-0.0052	-0.0063	-0.0096	-0.0096
1.0	0.0005		-0.0002	-0.0005	-0.0004	0.0014	-0.0011	-0.0072	-0.0085	-0.0126	-0.0128
	0.01		-0.0009	-0.0034	-0.0040	-0.0031	-0.0114	-0.0293	-0.0333	-0.0465	-0.0483
Analog	0	0.20	-0.0001	-0.0004	-0.0004	-0.0001	-0.0011	-0.0037	-0.0035	-0.0052	-0.0055
0	0.0001		-0.0001	-0.0003	-0.0004	-0.0002	-0.0011	-0.0031	-0.0035	-0.0052	-0.0054
	0.0005		-0.0001	-0.0003	-0.0003	-0.0002	-0.0009	-0.0023	-0.0032	-0.0047	-0.0049
	0.001		-0.00002	-0.0002	-0.0005	-0.0002	-0.0015	-0.0028	-0.0053	-0.0016	-0.0048
0.5	0.0005		-0.00008	-0.00031	-0.00038	-0.00023	-0.00011	-0.0025	-0.0010	-0.0054	-0.0059
	0.0015*		-0.0001	-0.0003	-0.0003	-0.0001	-0.0010	-0.0027	-0.0031	-0.0046	-0.0048
	0.01		-0.0017	-0.0009	0.0006	-0.0001	-0.0010	-0.0029	-0.0033	-0.0049	-0.0051
1.0	0.0005		-0.0001	-0.0004	-0.0004	-0.0003	-0.0013	-0.0035	-0.0040	-0.0059	-0.0061
	0.01		-0.0003	-0.0013	-0.0015	-0.0017	-0.0045	-0.0108	-0.0122	-0.0178	-0.0188

*Data for $\gamma=0.5$, $\Delta\tau=0.0015$ taken at increment closest to τ.

Energy Balance for i^{th} Surface Node:

$$h(t_{f_i} - t_i)_\theta \, A_{f_i} + k\left[\sum_{j=1}^{4} \frac{r_{ij}}{\ell_{ij}}(t_j - t_i)_\theta\right] = \text{Net Energy In at Time } \theta$$

$$C_p \, \sigma \, (\text{Area})_i\left[\frac{dt_i}{d\theta}\right] = \text{Accumulation at Time } \theta$$

$$(\text{Area})_i = \text{Cross-Hatched Area}$$

Figure V-1. MacNeal's approximation for surface node on curved boundary with finite non-zero heat-transfer coefficient.
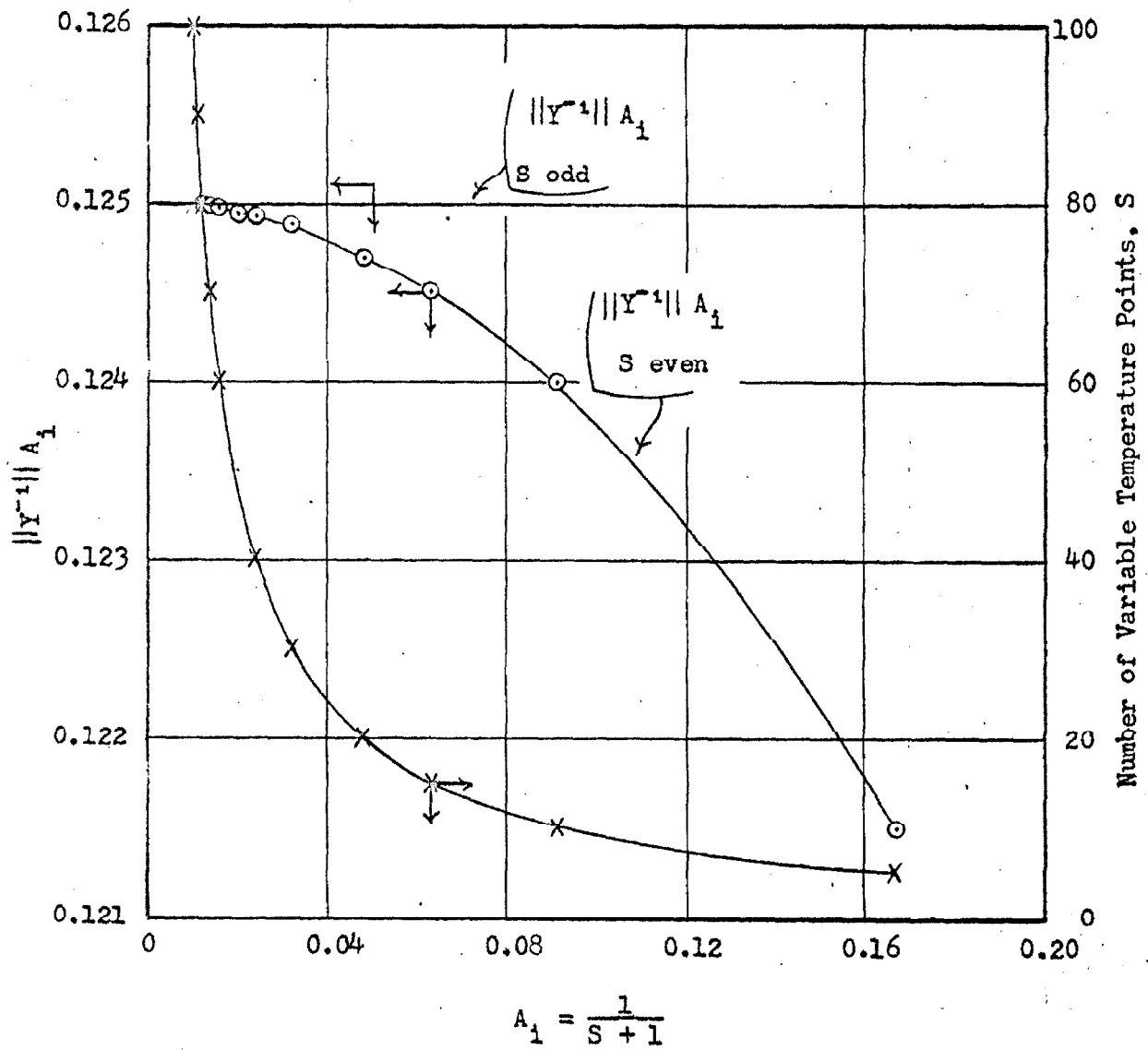
Figure V-2 . Relationship between nodal area and the product of the norm of the Y^{-1} matrix and the nodal area, one-dimensional problem, regular network; infinite h.

$$A_i = \frac{1}{S + S_1 + S_2 + 1}$$
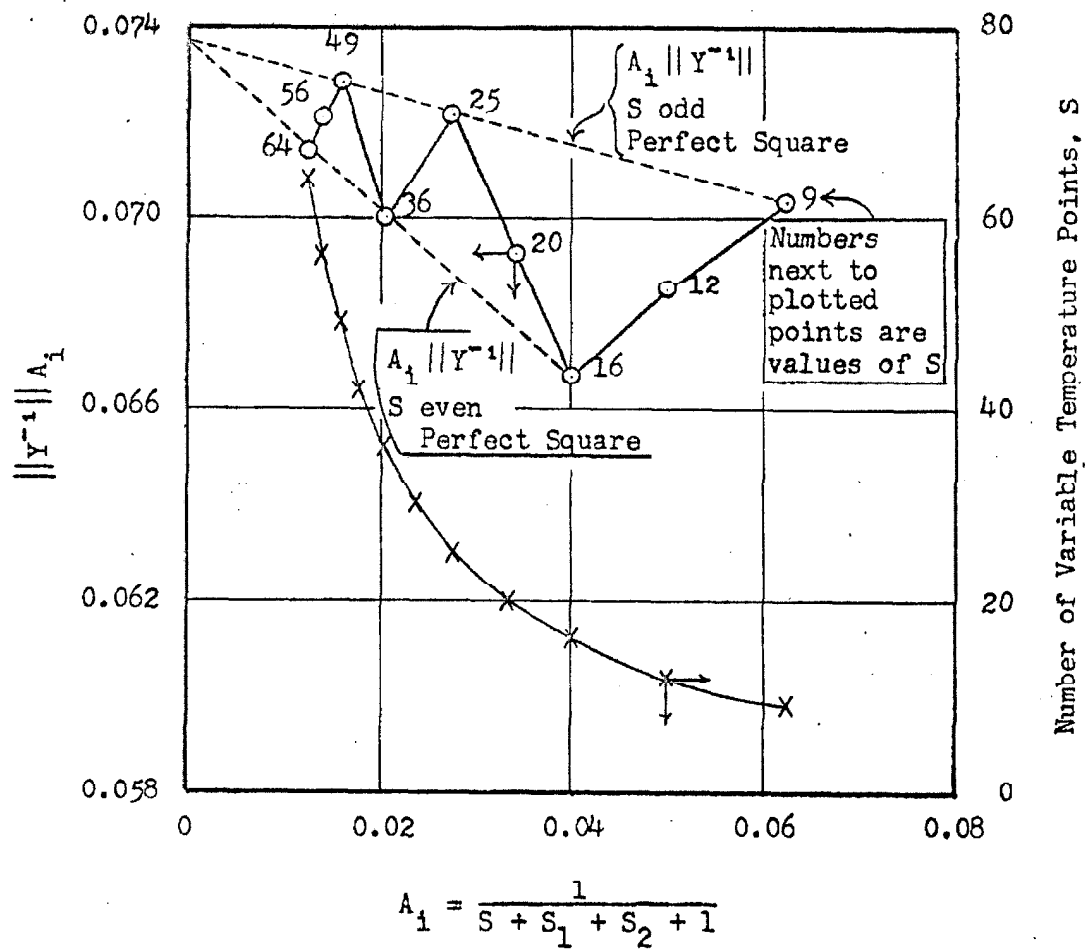
Figure V-3. Relationship between nodal area and the product
of the norm of the Y^{-1} matrix and the nodal area,
two-dimensional problem, regular rectangular
network; infinite h.
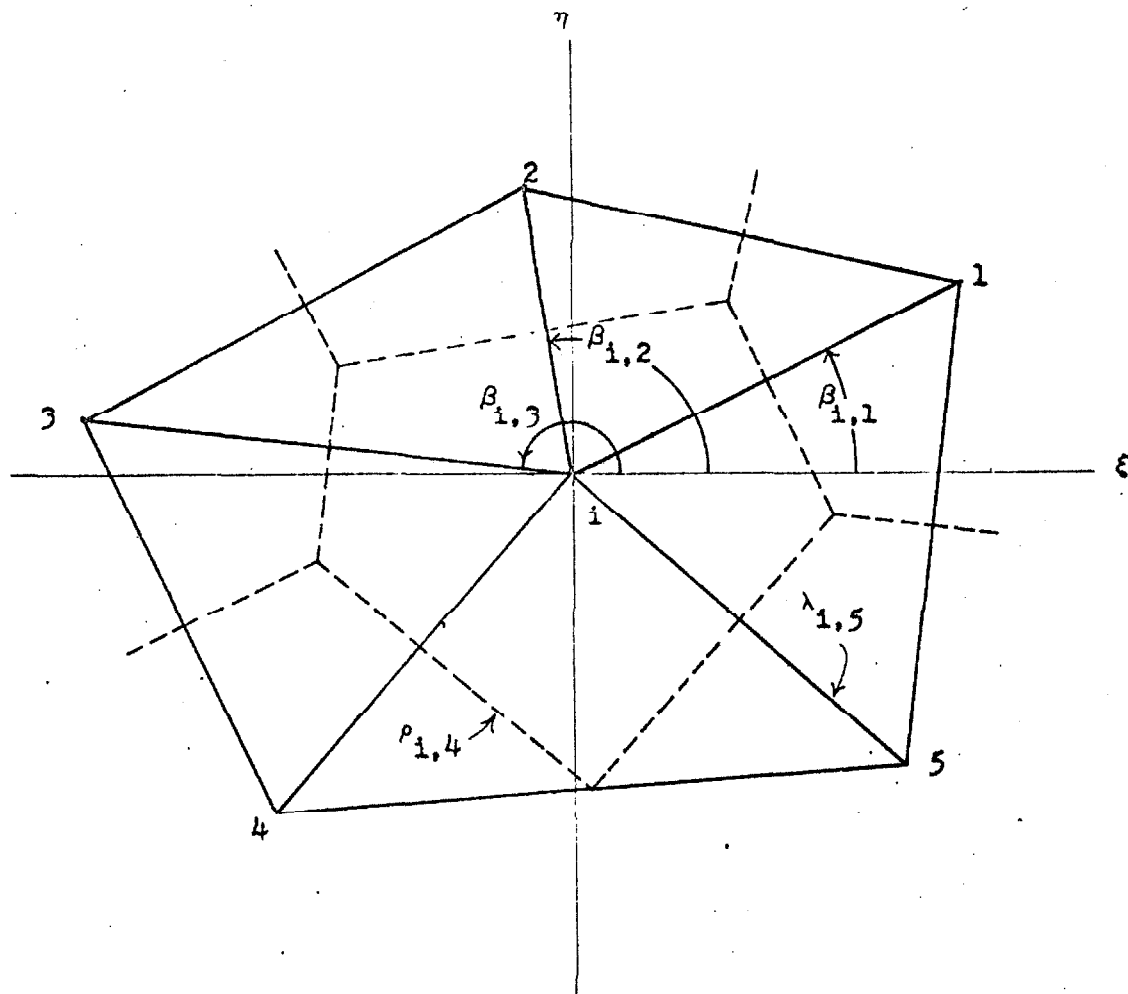
Figure V-4 . General asymmetric node, two-dimensional problem
showing geometry in dimensionless coordinates.
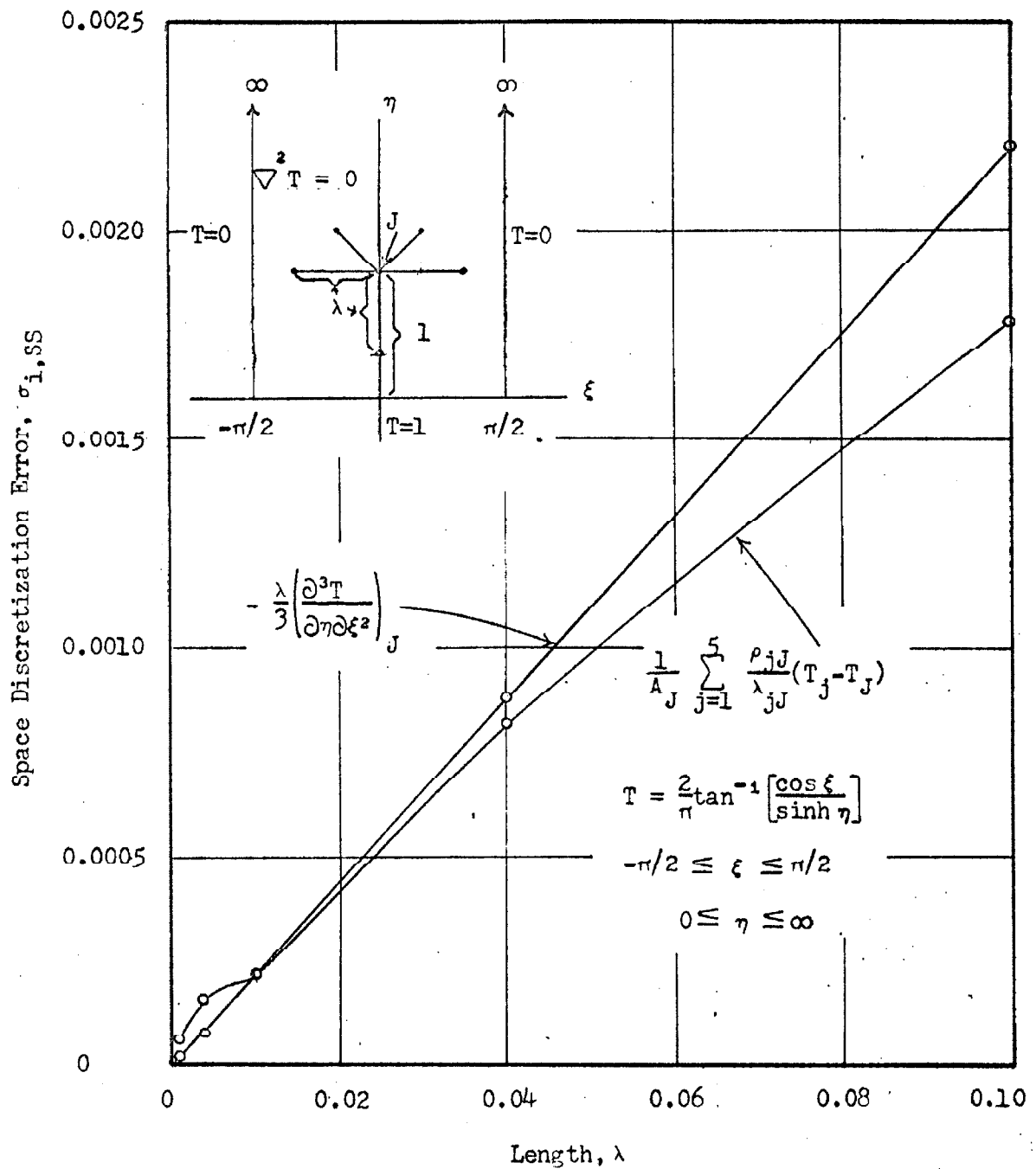
Figure V-5. Space discretization error, node J (see Table V-9), sequence of geometrically similar nodes.
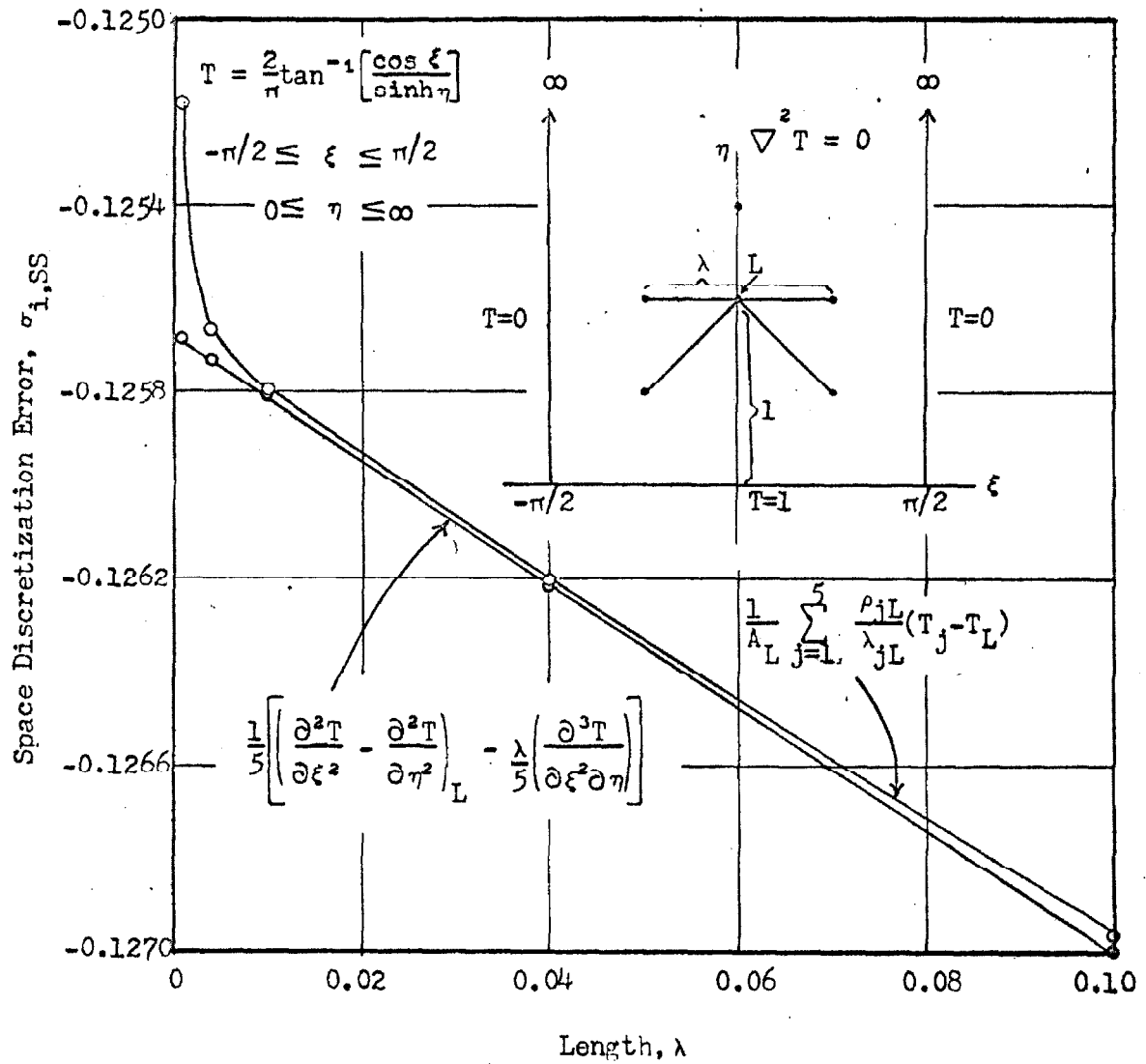
Figure V-6 . Space discretization error, node L (see Table V- 9), sequence of geometrically similar nodes.
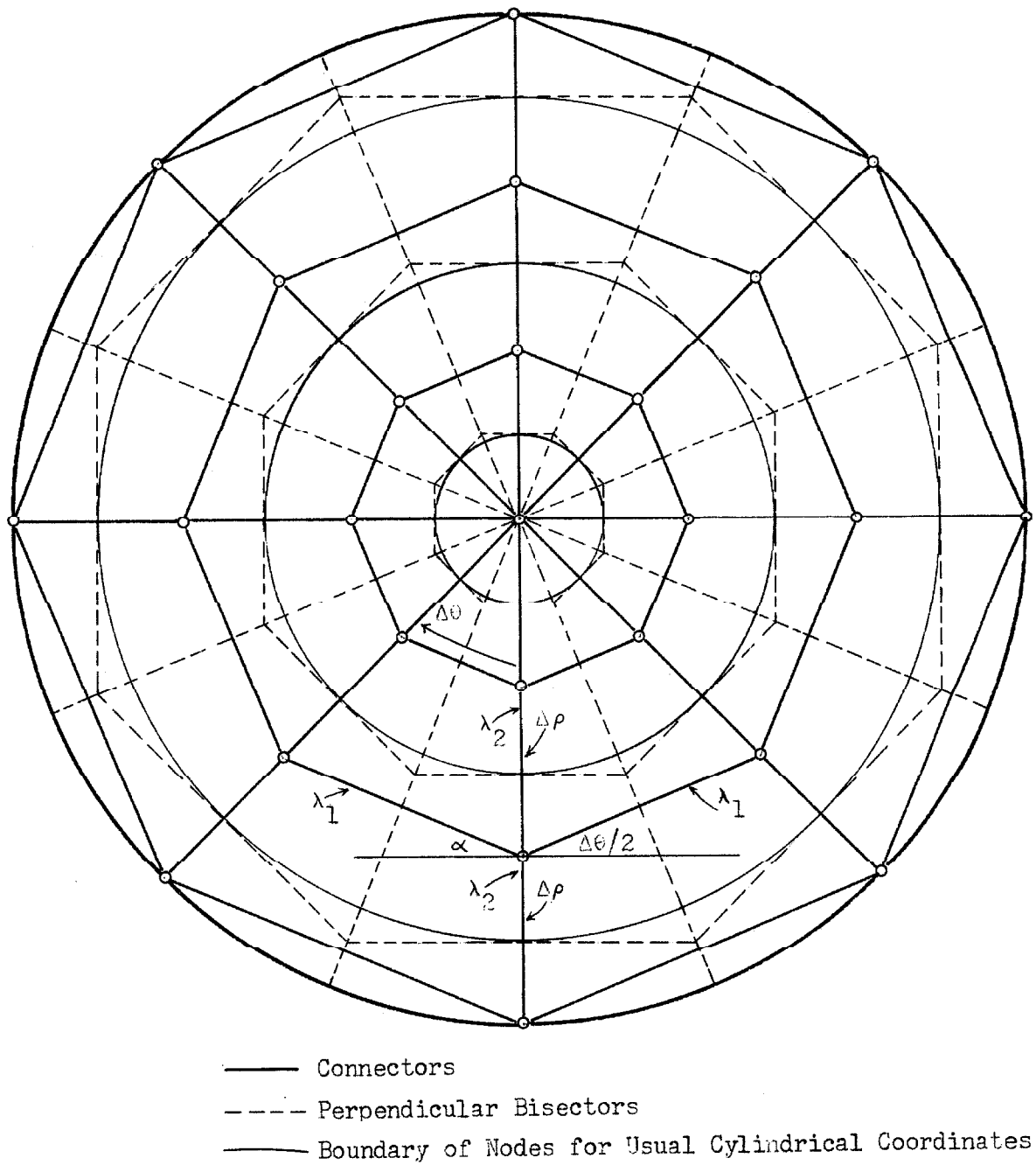
Figure V-7. Comparison between annular network and network of
trapezoidal nodes for cylindrical coordinates
based on MacNeal's rules; annular network is usual
approximation.
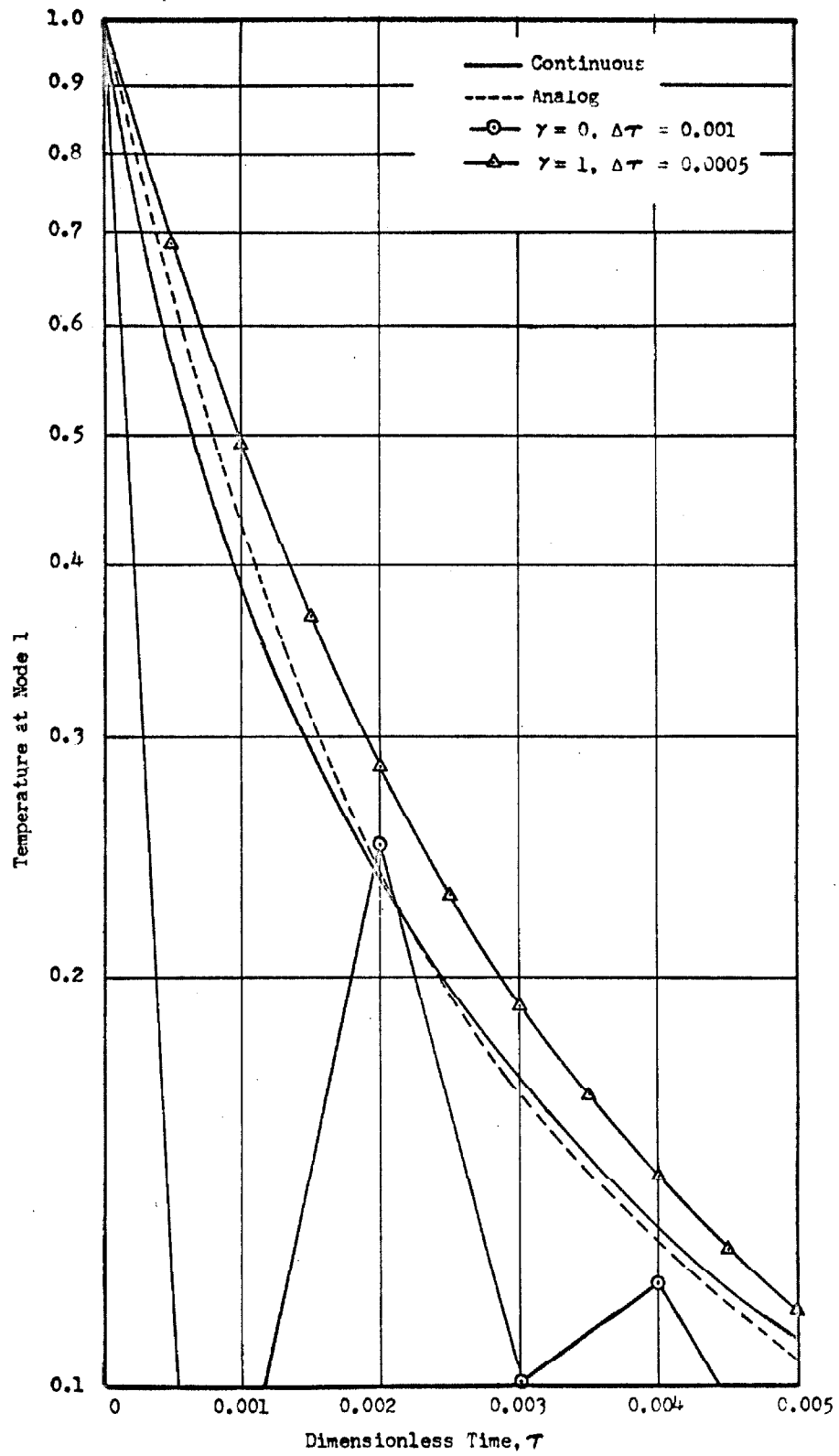
Figure V-8. Temperature at node 1 (Fig. III-1) versus
dimensionless time; short time.
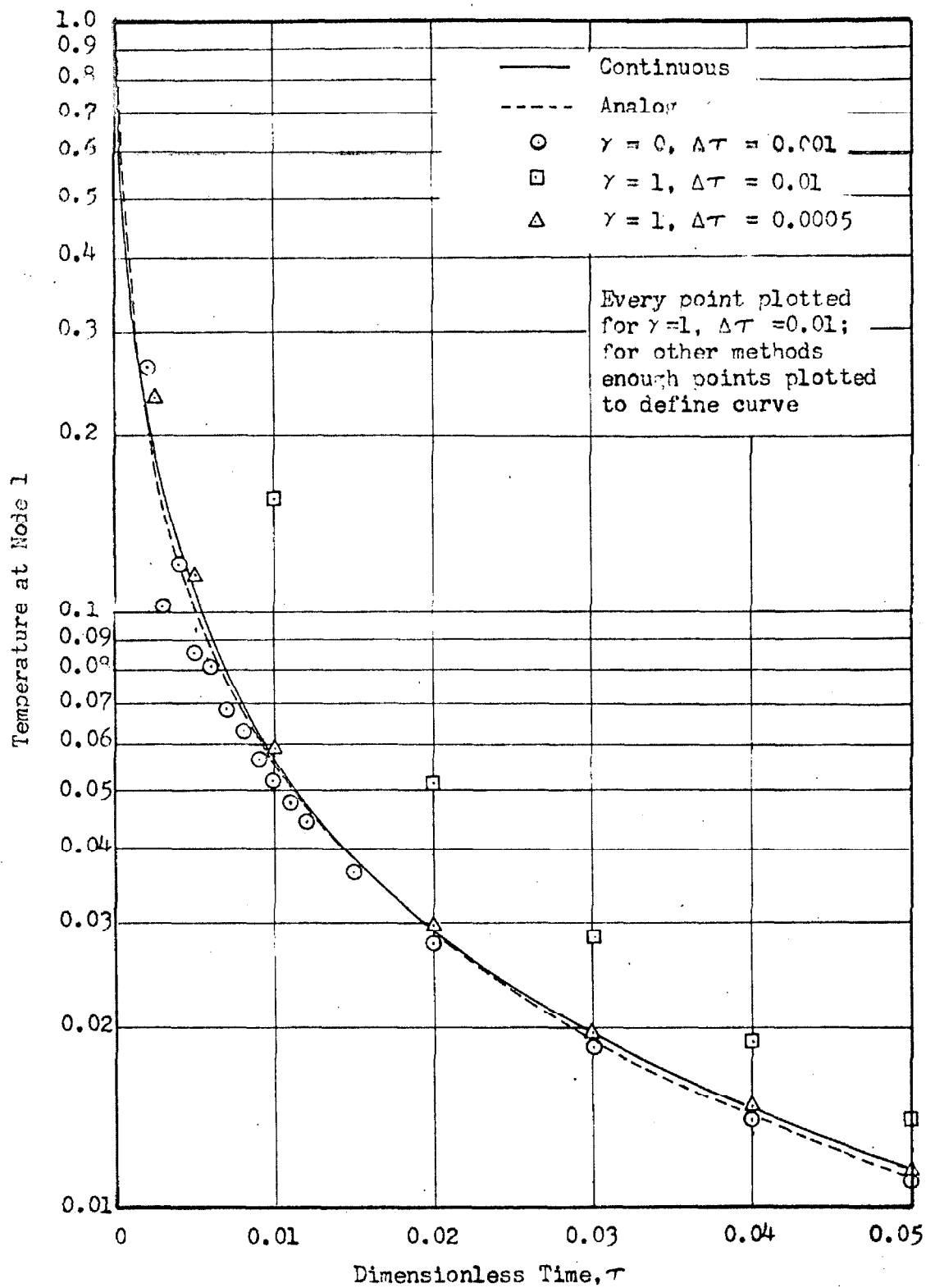
Figure V-9. Temperature at node 1 (Fig. III-1) versus dimensionless time; intermediate time.
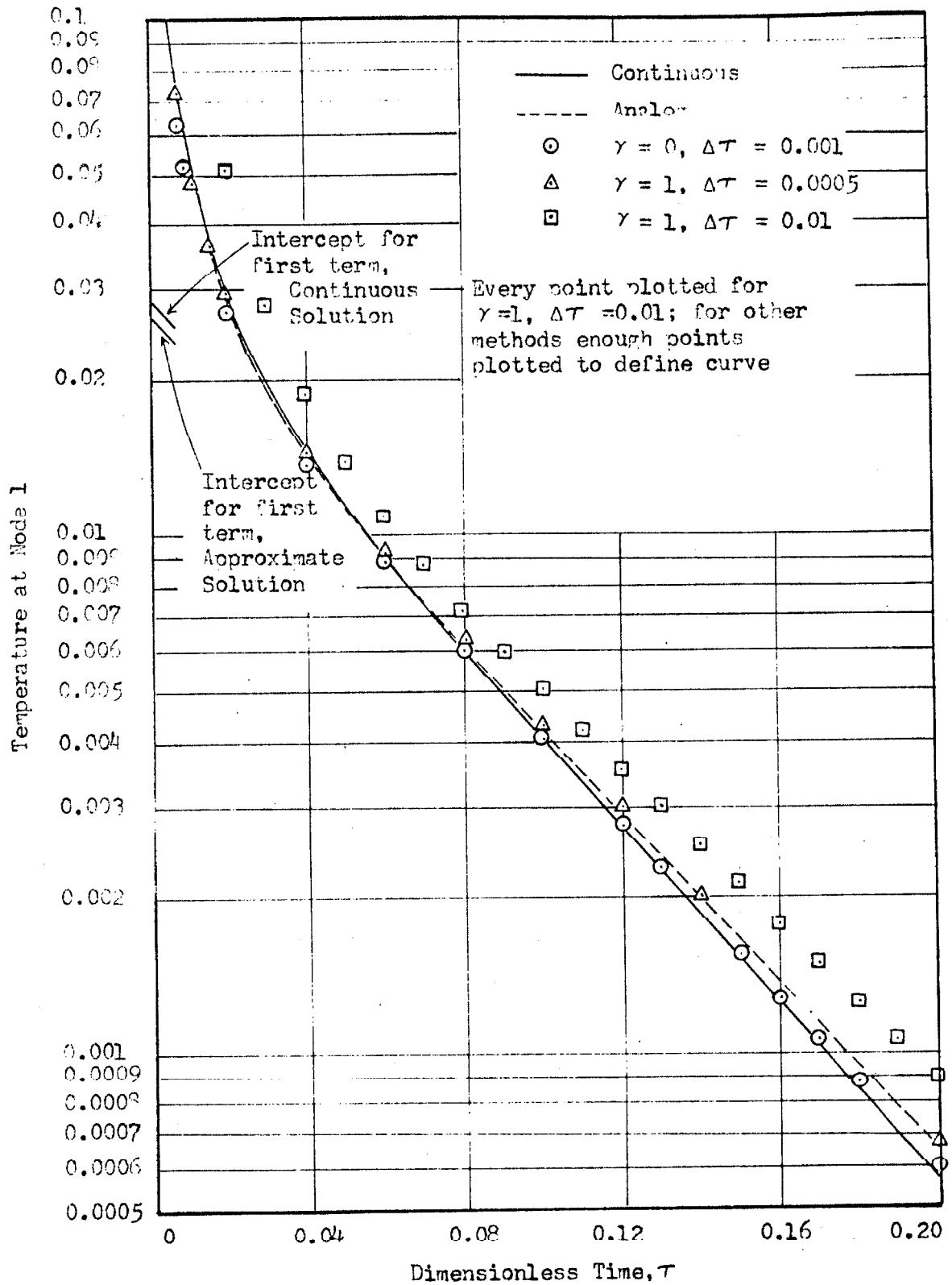
Figure V-10.   Temperature at node 1 (Fig. III-1) versus
dimensionless time; long time.

500
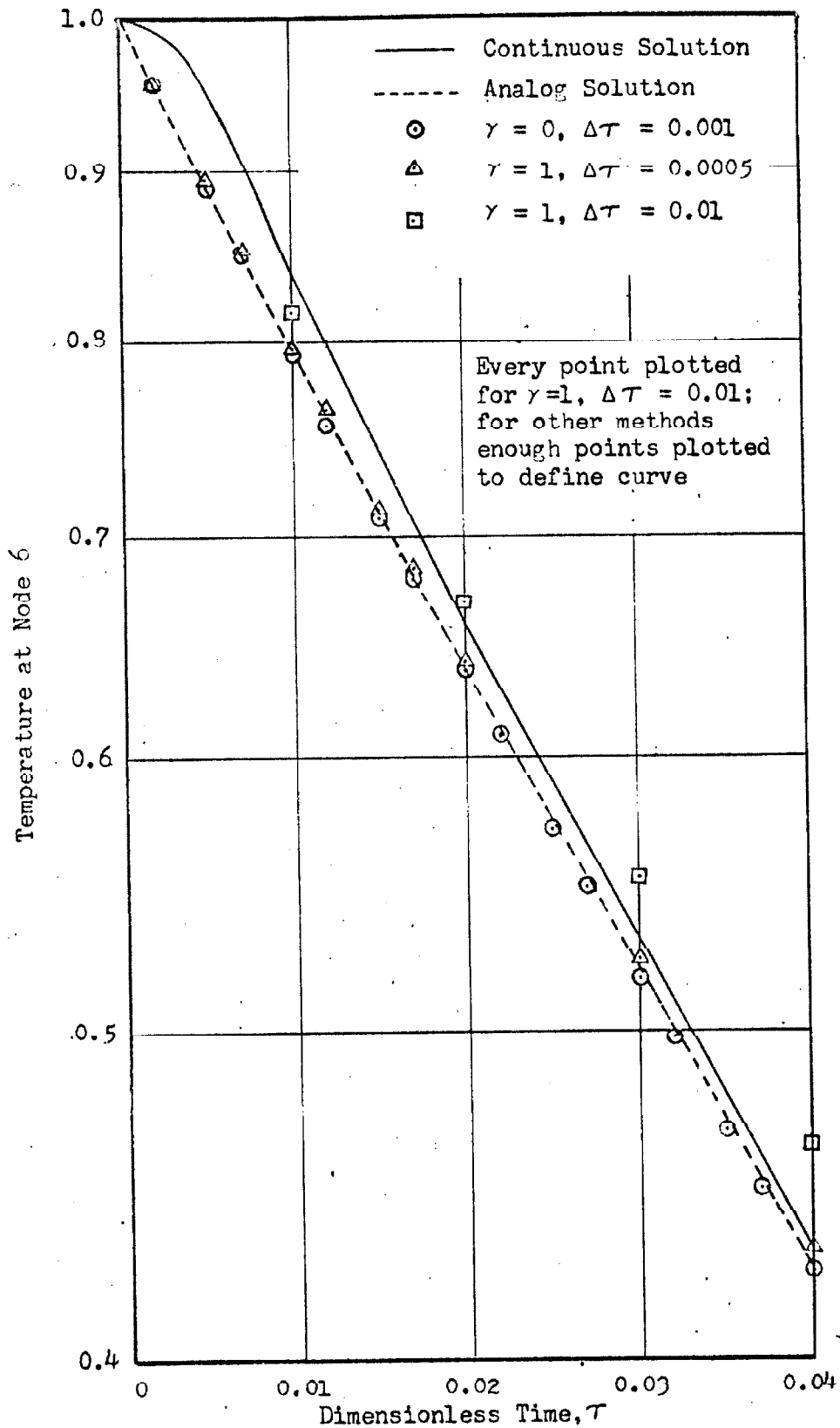
Figure V-11. Temperature at node 6 (Fig. III-1) versus
dimensionless time; short time.
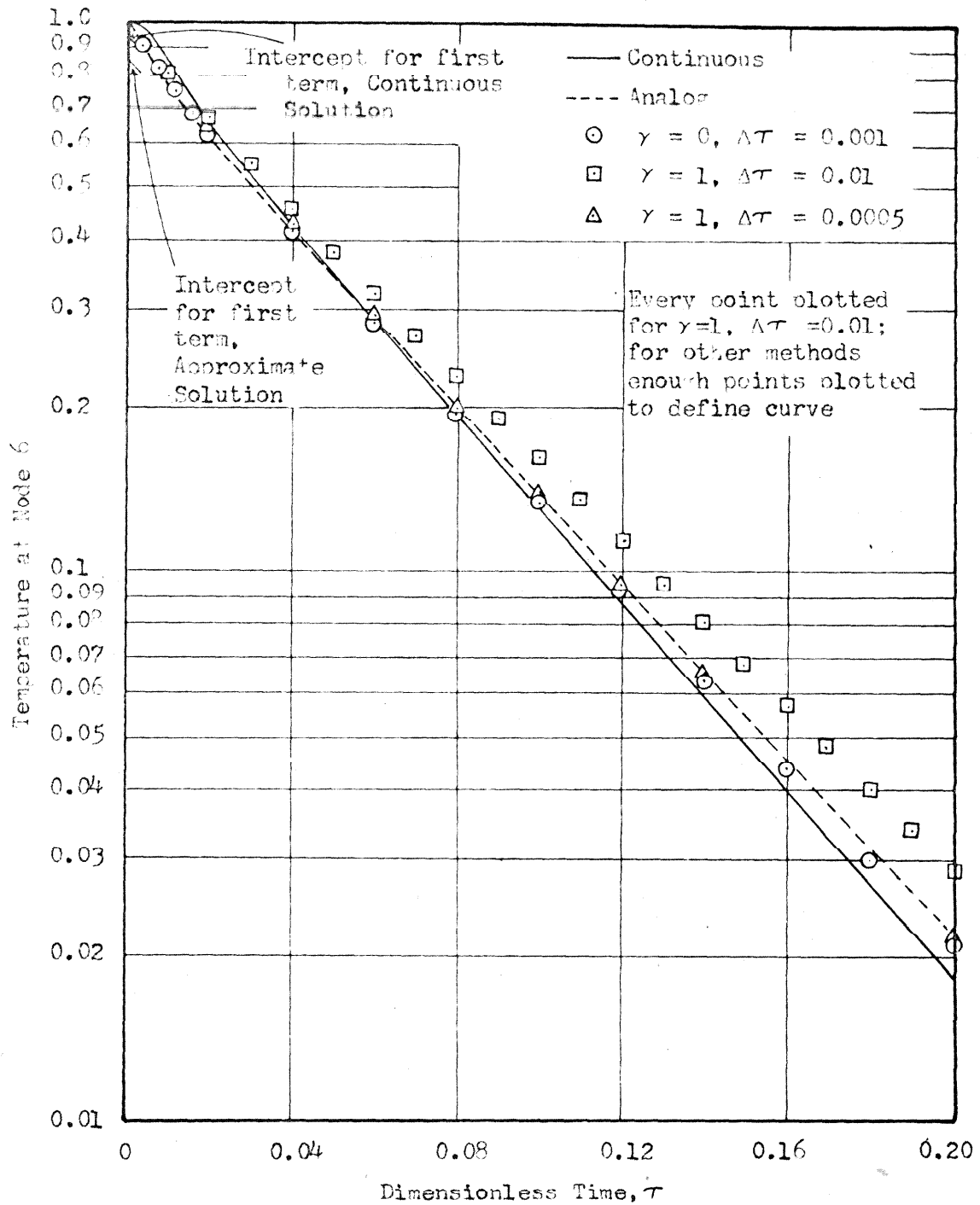
Figure V-12. Temperature at node 6 (Fig. III-1) versus
dimensionless time; long time.
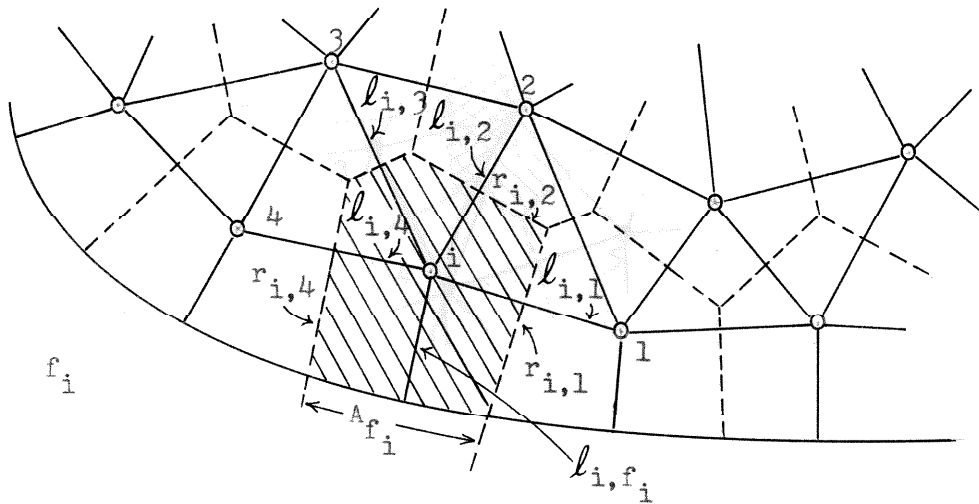
——— Connectors, Network Legs

----- Perpendicular Bisectors

Energy Balance for i^{th} Node:

$$\frac{A_{f_i}(t_{f_i}-t_i)_\theta}{\frac{1}{h}+\frac{\ell_{i,f_i}}{k}} + k\sum_{j=1}^{4}\frac{r_{ij}}{\ell_{ij}}(t_j-t_i)_\theta = \text{Net Energy in at Time}$$

$$C_p \sigma (Area)_i \frac{dt_i}{d\theta} = \text{Accumulation at Time}$$

$$(Area)_i = \text{Cross-Hatched Area}$$

$$t^*_{i,} = \text{Temperature at Boundary Surface of } i^{th} \text{ Adjacent Node}$$

$$h(t_{f_i}-t^*_i) = \frac{k(t_i-t_i)_\theta}{\ell_{i,f_i}}$$

$$\text{or} \quad t^*_{i_\theta} = \frac{\left[\frac{h\ell_{i,f_i}}{k}\left(t_{f_i}\right)+t_i\right]_\theta}{\frac{h\ell_{i,f_i}}{k}+1}$$

Figure V-13.   Modification to MacNeal's approximation for adjacent node on curved boundary with finite non-zero heat-transfer coefficient; analogous to mesh $\Delta\xi/2$.
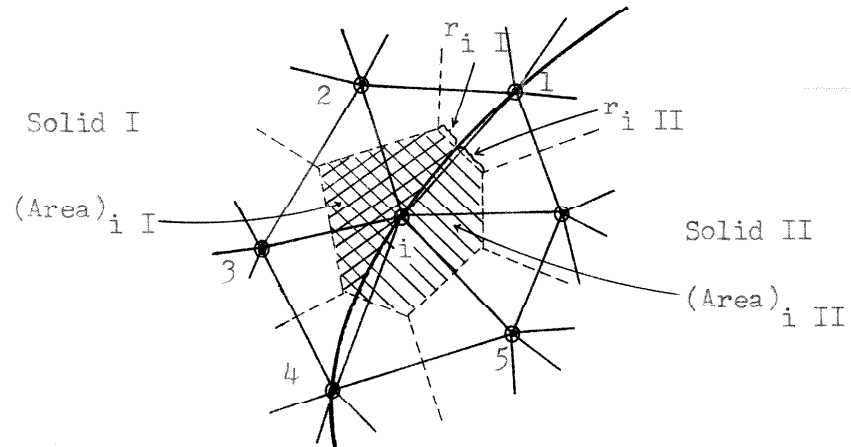
Dimensionless Capacity:

$$A_i = \left[(\text{Area})_{i\ I}\ C_{p\ I}\ \sigma_I + (\text{Area})_{i\ II}\ C_{p\ II}\ \sigma_{II} \right] \frac{1}{C_{p\ 0}\ \sigma_0 L^2}$$

Dimensionless Conductance:

$$y_{i\ I} = \frac{1}{k_0} \left(k_I r_{i\ I} + k_{II} r_{i\ II} \right)$$

MacNeal Interfacial Node

Figure V-14. MacNeal node for interfacial boundaries between
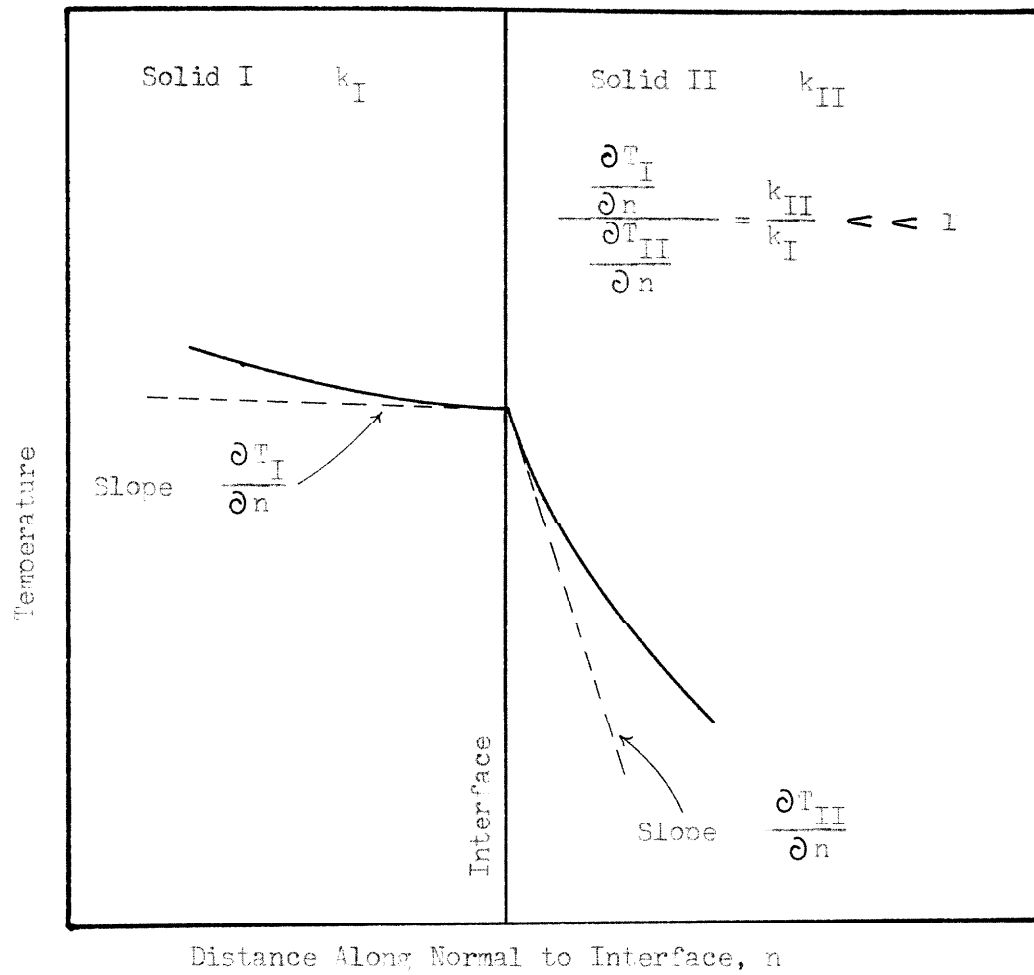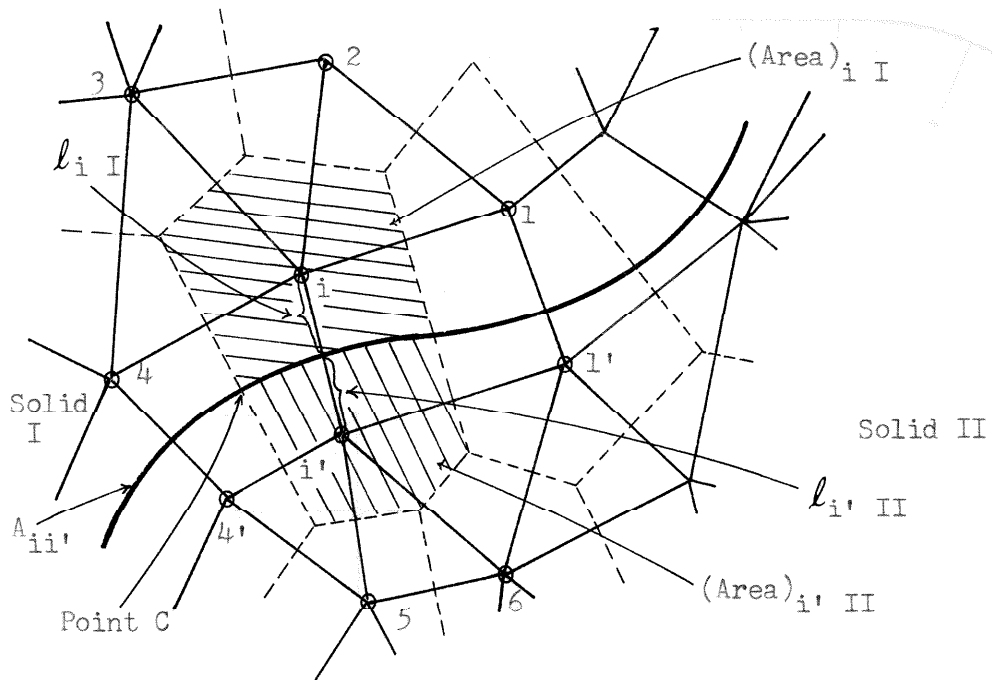uniform solids of different thermal properties.

Figure V-15. Continuous temperature distribution across interfacial boundary of uniform solids with very different thermal properties.
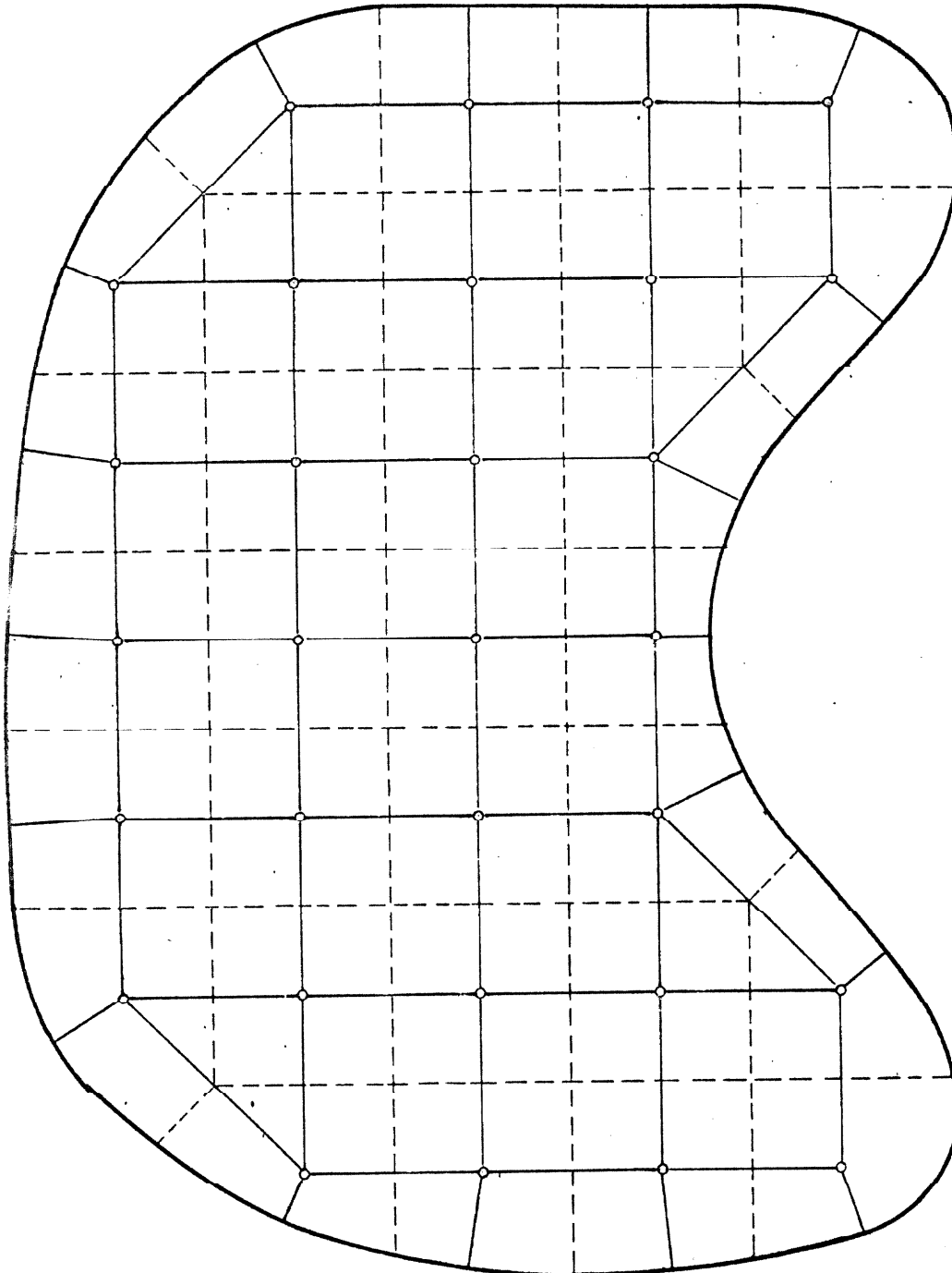
$$A_{i\ I} = \frac{C_{p\ I}\ \sigma_I\ (\text{Area})_{i\ I}}{C_{p\ 0}\ \sigma_0 L^2}$$

$$A_{i'\ II} = \frac{C_{p\ II}\ \sigma_{II}\ (\text{Area})_{i'\ II}}{C_{p\ 0}\ \sigma_0 L^2}$$

$$y_{ii'} = \frac{A_{ii'}}{k_0} \left[\frac{1}{\dfrac{\ell_{i\ I}}{k_I} + \dfrac{\ell_{i'\ II}}{k_{II}}} \right]$$
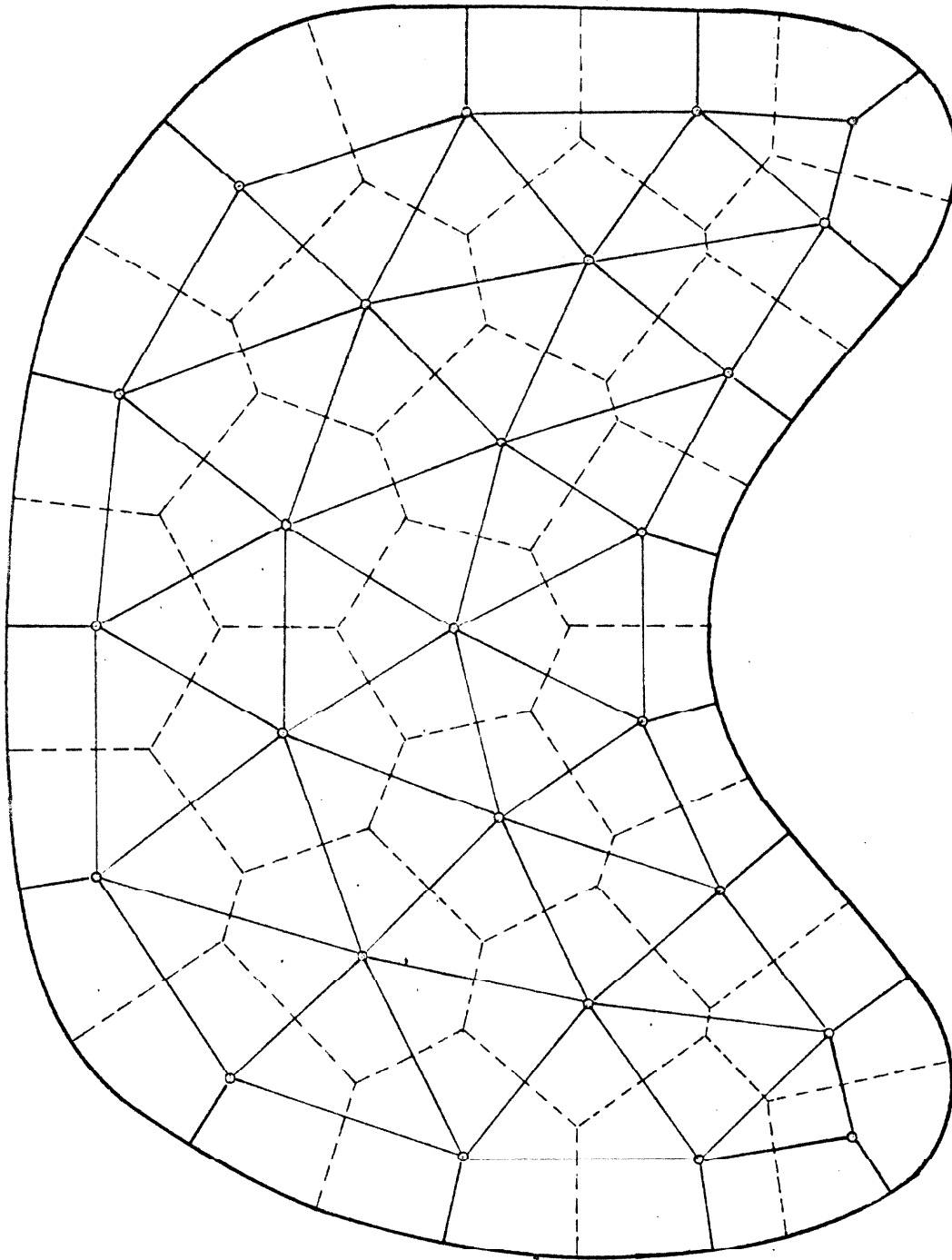
(Other conductances in similar fashion)

Figure V-16. Modified nodes for interfacial boundaries between uniform solids of different thermal properties.

Number of Adjacent Nodes: 18
Number of Interior Nodes: 12
Total Number of Nodes: 30

Figure V-17.   Network to approximate solid with curved boundary;
uses only square interior nodes.

Number of Adjacent Nodes   17
Number of Interior Nodes   9
Total Number of Nodes   26

Figure V-18.   Network to approximate solid with curved boundary;
distorted triangular network of distorted
hexagonal nodes.